LIN37-DREAM Prevents DNA End Resection and Homologous Recombination at DNA Double Strand Breaks in Quiescent Cells

Bo-Ruei Chen[1,2], Yinan Wang[3], Anthony T. Tubbs[4], Dali Zong[4], Faith C. Fowler[3], Nicholas Zolnerowich[4], Wei Wu[4], Amelia Bennett[3], Chun-Chin Chen[3], Wendy Feng[1], Andre Nussenzweig[4], Jessica K. Tyler[3,*], Barry P. Sleckman[1,2,*].

[1]Division of Hematology and Oncology, [2]O'Neal Comprehensive Cancer Center, University of Alabama at Birmingham, Birmingham, AL 35233. [3]Department of Pathology and Laboratory Medicine, Weill Cornell Medicine, New York, NY 10065. [4]Laboratory of Genome Integrity, National Cancer Institute, Bethesda, MD 20892.

*Correspondence to: Barry P. Sleckman, MD, PhD,
O'Neal Comprehensive Cancer Center at UAB
1720 2nd Avenue South, WTI 202
Birmingham, AL 35294-3300
bps@uab.edu

Jessica K. Tyler, PhD
Department of Pathology and Laboratory Medicine
Weill Cornell Medicine
1300 York Avenue
New York, NY
jet2021@med.cornell.edu

Abstract

DNA double strand break (DSB) repair by homologous recombination (HR) is thought to be restricted to the S- and G_2- phases of the cell cycle in part due to 53BP1 antagonizing DNA end resection in G_1-phase and non-cycling quiescent (G_0) cells. Here, we show that LIN37, a component of the DREAM transcriptional repressor, functions in a 53BP1-independent manner to prevent DNA end resection and HR in G_0 cells. Loss of LIN37 leads to expression of HR proteins, including BRCA1, BRCA2, PALB2 and RAD51, and DNA end resection in G_0 cells even in the presence of 53BP1. In contrast to 53BP1-deficiency, DNA end resection in LIN37-deficient G_0 cells depends on BRCA1 and leads to RAD51 filament formation and HR. LIN37 is not required to protect DNA ends in cycling cells at G_1-phase. Thus, LIN37 regulates a novel 53BP1-independent cell phase-specific DNA end protection pathway that functions uniquely in quiescent cells.

Introduction

DNA double strand breaks (DSBs) are repaired by two main pathways, non-homologous end joining (NHEJ) and homologous recombination (HR) (Prakash et al. 2015, Chang et al. 2017). HR functions in the S- and G_2-phases of the cell cycle using the sister chromatid as a template for precise homology-directed repair of DSBs. In contrast, NHEJ functions in all phases of the cell cycle to rejoin broken DNA ends and is the only pathway of DSB repair in G_1-phase cells and in non-cycling cells that have exited the cell cycle and are quiescent in G_0, which comprise the majority of cells in the human body (Chang et al. 2017). The initiation of HR requires DNA end resection to generate extended single stranded DNA (ssDNA) overhangs that are coated by the trimeric ssDNA binding protein complex RPA1/2/3 (hereafter referred to as RPA) (Ciccia and Elledge 2010). RPA is subsequently replaced by RAD51, and the RAD51 nucleofilament mediates a search for a homologous template usually within the sister chromatid to enable the completion of HR-mediated DNA DSB repair (Mimitou and Symington 2009, Wyman, Ristic, and Kanaar 2004). In contrast, NHEJ works best on DNA ends with minimal ssDNA overhangs, necessitating that DNA end resection be limited in G_1-phase and G_0 cells (Chang et al. 2017, Symington and Gautier 2011). Extensive resection and ssDNA generation at broken DNA ends in cells at G_0/G_1 would antagonize NHEJ-mediated DSB repair and promote aberrant homology-mediated repair, due to the absence of

sister chromatids, forming chromosomal translocations and deletions leading to genome instability (Ciccia and Elledge 2010). Therefore, the generation of ssDNA at broken DNA ends is the critical decision point for whether a DSB will be repaired by NHEJ and HR. As such, highly regulated processes that control DNA end resection are critical for ensuring appropriate choice of DSB repair pathways in all cells.

During HR, BRCA1 initiates the resection of broken DNA ends with the CTIP and MRE11 nucleases generating short ssDNA tracts that are extended by the nucleases such as EXO1 and DNA2-BLM (Symington and Gautier 2011). Other proteins, including Fanconi Anemia proteins such as FANCD2, are also involved in regulating DNA end resection (Unno et al. 2014, Murina et al. 2014, Cai et al. 2020). In cells where NHEJ must repair DSBs, the extensive resection of DNA ends must be prevented and 53BP1 and its downstream effectors RIF1 and the shieldin complex antagonize DNA end resection in these cells (Setiaputra and Durocher 2019, Mirman and de Lange 2020, Bunting et al. 2010). 53BP1 and shieldin may protect DNA ends by inhibiting the recruitment or activity of pro-resection proteins and also by promoting DNA synthesis at resected DNA ends to “fill in” the ssDNA gap generated by resection (Mirman and de Lange 2020, Setiaputra and Durocher 2019).

Whether pathways exist in addition to 53BP1 and RIF1/shieldin that protect DNA ends and promote genome integrity by preventing aberrant homology-mediated DSB repair is unclear. Here we develop an unbiased whole genome CRISPR/Cas9 screening approach based on assaying RPA loading at DSBs to identify genes encoding proteins that prevent DNA end resection and ssDNA generation in cells with 2N DNA content, which will be in either G_0 or G_1. This approach identified gRNAs targeting genes encoding proteins known to protect DNA ends such as 53BP1 and RIF1. However, this screen also identified LIN37, a protein not known to function in DNA end processing and DSB repair. LIN37 is a component of the DREAM (dimerization partner, RB-like, E2F and multi-vulval) transcriptional repressor complex (Litovchick et al. 2007, Sadasivam and DeCaprio 2013, Mages et al. 2017). Here we show that LIN37 functions in a 53BP1-independent manner to protect DNA ends from resection exclusively in quiescent G_0 cells. Moreover, while loss of either 53BP1 or LIN37 leads to loading of RPA at DSBs in G_0 cells, loss of LIN37 further leads to subsequent steps of HR including RAD51 loading and homology-mediated DSB repair.

Results

Identification of novel factors that regulate DNA end resection: Murine pre-B cells transformed with the Abelson murine leukemia virus kinase, hereafter referred to as abl pre-B cells, are rapidly cycling cells (Rosenberg, Baltimore, and Scher 1975). When treated with the abl kinase inhibitor, imatinib, abl pre-B cells stop cycling with a predominantly 2N DNA content indicative of them being in G_0/G_1 (Bredemeyer et al. 2006, Muljo and Schlissel 2003). Imatinib treated abl pre-B cells that ectopically express Bcl2 survive in culture for several days and we refer to these cells as non-cycling abl pre-B cells (Bredemeyer et al. 2006).

DNA DSBs in G_0/G_1 cells are repaired by NHEJ, which requires DNA Ligase 4 to join the broken DNA ends (Chang et al. 2017). Consequently, DNA DSBs generated in non-cycling DNA Ligase 4-deficient (*Lig4*$^{-/-}$) abl pre-B cells persist un-repaired (Helmink et al. 2011). These persistent DSBs are protected from nucleolytic activity and exhibit minimal DNA end resection (Tubbs et al. 2014, Dorsett et al. 2014, Helmink et al. 2011). However, loss of H2AX or 53BP1 in abl pre-B cells leads to extensive DNA end resection and the generation of ssDNA overhangs (Tubbs et al. 2014, Dorsett et al. 2014, Helmink et al. 2011). ssDNA at resected DNA ends binds to RPA, which can be assayed by flow cytometry after detergent extraction of soluble RPA (Forment, Walker, and

126 Jackson 2012). Indeed, as compared to non-cycling *Lig4*$^{-/-}$ abl pre-B cells, the
127 generation of DSBs by ionizing radiation (IR) in non-cycling *Lig4*$^{-/-}$*:53bp1*$^{-/-}$ abl
128 pre-B cells led to robust chromatin-associated RPA as assayed by flow
129 cytometry (Figure 1A). This assay detects more extensive DNA end resection
130 in the absence of 53BP1 and thus serves as the basis for a screen to identify
131 additional proteins that normally function to prevent extensive DNA end
132 resection in G_0/G_1 cells.
133
134 To facilitate our screen for gRNAs that increase association of RPA with DSBs,
135 we introduced a lentivirus containing a FLAG-Cas9 cDNA under control of a
136 doxycycline-inducible promoter into *Lig4*$^{-/-}$ abl pre-B cells. Immunodetection of
137 the FLAG epitope allowed flow cytometric assessment of FLAG-Cas9 protein
138 expression upon doxycycline treatment, showing that FLAG-Cas9 can be
139 induced in all the cells in the population (Figure 1B). A lentiviral mouse guide
140 RNA (gRNA) library containing approximately 90,000 gRNAs to 18,000 mouse
141 genes was introduced into these cells followed by doxycycline treatment for
142 seven days to promote Cas9-gRNA-mediated gene inactivation (Figure 1C)
143 (Tzelepis et al. 2016). After 2 days of imatinib treatment to render these cells
144 non-cycling, the cells were subjected to irradiation (IR) and those with the
145 highest level (top 10%) of chromatin-bound RPA were isolated by flow
146 cytometric cell sorting (Figure 1C). The gRNAs from this “RPA-high” cell

147 population were sequenced, and the frequency of individual gRNAs in the RPA-
148 high population relative to those in the “RPA-low” population was determined.
149
150 Multiple gRNAs to genes encoding proteins known to prevent DNA end
151 resection such as 53BP1, RIF1 and shieldin subunits were enriched in the RPA-
152 high cell population, demonstrating the veracity of this screening approach
153 (Figure 1D and Table S1). In addition, several gRNAs to *Lin37*, a gene encoding
154 the LIN37 subunit of the MuvB complex were also highly enriched in RPA-high
155 cells (Figure 1D and Table S1) (Litovchick et al. 2007). When bound to the
156 pocket proteins p130/p107, and E2F proteins E2F4/5 and DP, the MuvB
157 complex forms the DREAM transcription repressor complex, which functions to
158 repress genes that promote entry into the cell cycle (Litovchick et al. 2007,
159 Sadasivam and DeCaprio 2013, Mages et al. 2017).
160
161 **RPA accumulation at DNA DSBs in non-cycling LIN37-deficient cells:** To
162 validate the hit from the gRNA screen, we generated DNA Ligase 4-deficient
163 abl pre-B cells that were deficient in LIN37 (*Lig4*$^{-/-}$*:Lin37*$^{-/-}$) (Figure 2A). Similar
164 to 53BP1-deficient abl pre-B cells, LIN37-deficienct cells also exhibited
165 increased RPA association with DSBs in chromatin after IR, with most of the
166 cells lacking LIN37 having even more chromatin bound RPA after IR than cells
167 lacking 53BP1 (Figure 2B). This is not a consequence of more DNA damage

168 occurring in the absence of LIN37, because all the cells had similar levels of
169 γH2AX indicative of similar DNA DSB generation in response to IR (Figure 2B).
170 Analyses of non-cycling wild type (*WT*), *53bp1*$^{-/-}$ and *Lin37*$^{-/-}$ abl pre-B cells that
171 expressed Ligase 4 yielded similar results, indicating that RPA binding at DSBs
172 in 53BP1 and LIN37 deficient abl pre-B cells does not depend on DNA Ligase
173 4 deficiency (Figure S1).
174
175 LIN37 is a component of the DREAM complex, which along with Rb prevents
176 cells from entering S-phase where resection of DNA ends and RPA loading
177 normally occur at DSBs as part of HR (Weinberg 1995, Sadasivam and
178 DeCaprio 2013, Ciccia and Elledge 2010). However, loss of LIN37 does not
179 cause imatinib-treated abl pre-B cells to enter S-phase as evidenced by
180 imatinib-treated *Lig4*$^{-/-}$*:Lin37*$^{-/-}$ abl pre-B cells having primarily 2N DNA content
181 and not incorporating BrdU, which would be indicative of DNA synthesis in S-
182 phase cells (Figure 2C). If RPA is binding to chromatin at DSBs this binding
183 should form discrete RPA IR-induced foci (IRIF) that can be visualized by
184 immunofluorescence staining. Indeed, chromatin-bound RPA in IR treated non-
185 cycling *Lig4*$^{-/-}$*:53bp1*$^{-/-}$ and *Lig4*$^{-/-}$*:Lin37*$^{-/-}$ abl pre-B cells formed discrete nuclear
186 foci indicative of localization at DSBs (Figure 2D).
187

188 To evaluate LIN37 function in a different cell type using a distinct approach to
189 render them non-cycling we generated LIN37- and 53BP1-deficient MCF10A
190 human mammary epithelial cells. Upon withdrawal of epidermal growth factor
191 (EGF) these cells stop cycling and have 2N DNA content and lack of BrdU
192 incorporation consistent with the notion that they are in G_1/G_0 (Figures 2E and
193 2F). Non-cycling *LIN37*$^{-/-}$ and *53BP1*$^{-/-}$ MCF10A cells also exhibited increased
194 chromatin-bound RPA after IR as compared to wild type MCF10A cells (Figures
195 2G and 2H), indicating that the function of LIN37 in suppressing RPA
196 accumulation at DNA DSBs in non-cycling cells is conserved in human and
197 mouse. As was seen above in the mouse cells, the extent of RPA accumulation
198 in human cells lacking LIN37 after IR was greater than seen in cells lacking
199 53BP1, suggesting that LIN37 plays an important role in preventing DNA end
200 resection and extensive generation of ssDNA at DSBs in non-cycling
201 mammalian cells (Fig. 2G, 2H).
202
203 **DNA ends are resected in non-cycling LIN37-deficient cells**: The CTIP
204 nuclease is required to initiate DNA end resection during HR and DNA ends in
205 non-cycling abl pre-B cells that are deficient in H2AX undergo resection that
206 depends on CTIP (Sartori et al. 2007, Helmink et al. 2011). To determine
207 whether IR-induced RPA association with chromatin in LIN37-deficient abl pre-
208 B cells also depends on CTIP, *Lig4*$^{-/-}$*:53bp1*$^{-/-}$ and *Lig4*$^{-/-}$*:Lin37*$^{-/-}$ abl pre-B cells

209 that expressed a *Ctip* gRNA were treated with doxycycline to induce Cas9
210 expression and maximal CTIP protein reduction, due to *Ctip* gene inactivation,
211 prior to analysis (Figure 3A). This approach, which we refer to as "bulk gene
212 inactivation", allows for the depletion of proteins normally required for cell
213 division and viability. The chromatin-bound RPA in IR treated non-cycling *Lig4*$^{-/-}$*:Lin37*$^{-/-}$
214 and *Lig4*$^{-/-}$*:53bp1*$^{-/-}$ abl pre-B cells depended on CTIP (Figure 3A),
215 indicating that the increased level of chromatin-bound RPA after IR in cells
216 lacking LIN37 or 53BP1 is due to DNA end resection that would lead to the
217 generation of ssDNA.
218
219 To gain direct evidence of DNA DSB end resection in LIN37-deficient abl pre-
220 B cells, DNA End Sequencing (End-seq) was used to directly assay DNA end
221 structures at approximately 200 *AsiSI* sites in abl pre-B cells with an inducible
222 *AsiSI* endonuclease (*iAsiSI*) (Canela et al. 2016). End-seq allows for nucleotide
223 resolution mapping of length and end position of DNA end resection at defined
224 DSBs induced by a variety of endonucleases (Canela et al. 2016). The End-
225 seq analysis revealed that that while *AsiSI* DSBs in non-cycling *Lig4*$^{-/-}$*:iAsiSI* abl
226 pre-B cells were minimally resected (<200bp), those in non-cycling *Lig4*$^{-/-}$*:Lin37*$^{-/-}$*:iAsiSI*
227 abl pre-B cells were resected up to 2 kb (Figures 3B and 3C). We
228 conclude that loss of LIN37 leads to the CTIP-dependent resection of broken
229 DNA ends in non-cycling cells.

LIN37 and 53BP1 are in distinct pathways of DNA end protection: 53BP1 and its downstream effector proteins protect DNA ends from resection through multiple potential mechanisms (Setiaputra and Durocher 2019, Mirman and de Lange 2020, Bunting et al. 2010). To determine whether LIN37 functions in the same pathway as 53BP1, we first examined whether loss of LIN37 alters the expression levels of key proteins in the 53BP1 pathway. In this regard, Western blotting revealed that loss of LIN37 did not lead to reduction in the levels of 53BP1, RIF1 or SHLD1 proteins in cycling or non-cycling abl pre-B cells (Figures 4A and S2A). Moreover, after IR treatment, robust and near equivalent numbers of 53BP1 and RIF1 foci form in non-cycling *Lig4*$^{-/-}$ and *Lig4*$^{-/-}$*:Lin37*$^{-/-}$ abl pre-B cells, demonstrating that both 53BP1 and RIF1 efficiently localize to DSBs in LIN37-deficient cells (Figures 34B, 4C, S2B and S2C).

To test genetically whether 53BP1 and LIN37 protects DNA ends using the same or different pathways, we conducted an epistasis analysis of DNA end resection in non-cycling cells lacking LIN37, 53PB1 or both of these proteins. To this end, a *Lin37* gRNA was used to carry out bulk *Lin37* inactivation in *Lig4*$^{-/-}$*:53bp1*$^{-/-}$ abl pre-B cells (Figure 4D). Loss of LIN37 in non-cycling *Lig4*$^{-/-}$*:53bp1*$^{-/-}$ abl pre-B cells led to an increase in chromatin-bound RPA after IR, as compared to non-cycling *Lig4*$^{-/-}$*:53bp1*$^{-/-}$ abl pre-B cells that express LIN37

(Figure 4D). Similarly, the loss of 53BP1 in non-cycling *Lig4*$^{-/-}$*:Lin37*$^{-/-}$ abl pre-B cells also led to increased chromatin-bound RPA after IR (Figure 4E). Given the additive effect of inactivation of both LIN37 and 53BP1, we conclude that in non-cycling cells 53BP1 and LIN37 are part of mechanistically distinct pathways that are both required to protect DNA ends from resection.

LIN37 suppresses the expression of DNA end resection and HR proteins in non-cycling cells: As LIN37 participates in the formation of the DREAM transcriptional repressor we considered the possibility that Lin37 may protect DNA ends through the suppression of genes encoding pro-resection proteins (Sadasivam and DeCaprio 2013). A mutant form of LIN37, LIN37^{CD}, does not associate with the DREAM complex and while DREAM lacking LIN37 binds to its target genes, it cannot repress their expression (Mages et al. 2017). To determine whether the resection of DNA ends depends on loss of DREAM transcription repressor activity, we assayed IR-induced RPA association with chromatin in non-cycling *Lig4*$^{-/-}$*:Lin37*$^{-/-}$ abl pre-B cells expressing WT LIN37 or DREAM-binding defective mutant, LIN37^{CD}. Expression of WT LIN37, but not LIN37^{CD}, in non-cycling *Lig4*$^{-/-}$*:Lin37*$^{-/-}$ abl pre-B cells decreased IR-induced chromatin-bound RPA (Figure 5A). That the extensive DNA end resection due to LIN37 deficiency cannot be rescued by expression of the LIN37 mutant that

271 is unable to assemble into the DREAM complex suggests that LIN37 functions
272 to protect DNA ends through its activity in the DREAM transcriptional repressor.
273
274 To identify genes repressed by DREAM that may suppress end resection in
275 non-cycling cells, we carried out RNA Seq analysis of cycling and non-cycling
276 *Lig4*$^{-/-}$ and *Lig4*$^{-/-}$*:Lin37*$^{-/-}$ abl pre-B cells. Cycling *Lig4*$^{-/-}$*:Lin37*$^{-/-}$ abl pre-B cells
277 exhibit very few (approximately 20) significant gene expression changes as
278 compared to *Lig4*$^{-/-}$ abl pre-B cells (Table S2). In contrast, when compared to
279 non-cycling *Lig4*$^{-/-}$ abl pre-B cells, non-cycling *Lig4*$^{-/-}$*:Lin37*$^{-/-}$ abl pre-B cells
280 exhibited increased expression (>3-fold) of over 300 genes (Figure 5B and
281 Table S2). We found that many genes up-regulated in non-cycling *Lig4*$^{-/-}$*:Lin37*$^{-}$
282 $^{/-}$ abl pre-B cells have functions in HR, including DNA end resection (*Brca1*,
283 *Bard1*, *Blm*, and *Exo1*), recombination (*Brca2*, *Bard1*, *Palb2*, *Mms22l*, *Rad51*,
284 *Rad51b*, and *Rad54b*) and DNA synthesis (*Hrob*/ *BC030867*, *Mcm3*, *Mcm4*,
285 *Mcm5*, *Mcm7*, *Mcm8*, *Pold1*, *Pole*). A subset of Fanconi Anemia (FA) genes
286 also exhibited increased expression in non-cycling *Lig4*$^{-/-}$*:Lin37*$^{-/-}$ abl pre-B cells
287 (Figure 5B and Table S2). These data indicate that in non-cycling abl pre-B
288 cells LIN37-DREAM transcriptionally represses many genes that function in
289 DNA end resection and HR.
290

Western blotting revealed that the levels of BRCA1, BARD1, BLM, RAD51 and FANCD2 proteins were extremely low in non-cycling *Lig4*$^{-/-}$ abl pre-B cells compared to cycling cells (Figure 5C). Consistent with their increased transcript levels, the protein levels of BRCA1, BARD1, BLM, RAD51 and FANCD2 were significantly elevated in non-cycling *Lin37*$^{-/-}$ and *Lig4*$^{-/-}$*:Lin37*$^{-/-}$ abl pre-B cells as compared to WT and *Lig4*$^{-/-}$ abl pre-B cells, respectively (Figures 5C and S3). In contrast, the levels of these proteins were not altered in cycling LIN37-deficient cells (Figures 5C and S3). The increased expression of these HR proteins was also observed in non-cycling, but not cycling, *Lin37*$^{-/-}$ human MCF10A cells, indicating that LIN37 represses the expression of key DNA end resection and HR proteins to potentially limit DNA end resection in both human and murine non-cycling cells (Figure 5D).

To determine whether the ability of LIN37 to repress expression of these key HR proteins in non-cycling cells required LIN37 to function in the context of the DREAM complex, we again used the LIN37^{CD} mutant which cannot form a transcriptionally repressive DREAM complex. We found that expression of wild type LIN37, but not LIN37^{CD} in non-cycling *Lig4*$^{-/-}$*:Lin37*$^{-/-}$ abl pre-B cells, led to a decrease in the levels of BRCA1, BARD1, BLM, RAD51 and FANCD2 proteins (Figure 5E). Of note is that the expression of the MRE11 and CTIP nucleases were not affected by loss of LIN37 in cycling or non-cycling cells

(Figures 5C and S3). We conclude that in non-cycling cells, LIN37, as part of the DREAM transcriptional repressor complex, represses genes encoding many proteins that function in DNA end resection and DSB repair by HR.

DNA resection and HR machinery are functional in non-cycling LIN37-deficienct cells: We performed another whole genome CRISPR/Cas9 reverse genetic screen to identify genes that mediate the extensive DNA end resection that occurs in non-cycling LIN37-deficient abl pre-B cells. To this end we identified gRNAs enriched in IR treated non-cycling *Lig4*$^{-/-}$*:Lin37*$^{-/-}$ abl pre-B cells that had low levels of chromatin-bound RPA, indicating reduced DNA end resection despite having no LIN37 (Table S3). As expected, gRNAs to *Rbbp8* (encodes CTIP) and to *Mre11b* (encodes MRE11) were enriched in these RPA low cells, in agreement with their nucleolytic roles in resection and emphasizing the validity of our screen (Table S3). In addition, we isolated gRNAs to many genes encoding DNA end resection and HR proteins that are normally repressed by LIN37, including *Brca1*, *Bard1*, *Blm* and several FA genes, indicating that the expression of these proteins brought about by LIN37-deficiency in non-cycling cells promotes the extensive DNA end resection that is observed in these cells (Table S3). Indeed, bulk inactivation of BRCA1, BARD1, BLM or FANCD2 significantly reduced the level of chromatin-bound RPA after IR in non-cycling *Lig4*$^{-/-}$*:Lin37*$^{-/-}$ abl pre-B cells (Figure 6A). In striking

contrast, the loss of these proteins had no effect on RPA localization to DSBs after IR treatment of non-cycling *Lig4*$^{-/-}$*:53bp1*$^{-/-}$ abl pre-B cells, further emphasizing that LIN37 and 53BP1 are part of mechanistically distinct pathways that prevent DNA end resection and ssDNA generation in non-cycling cells (Figures 6A).

LIN37-deficient non-cycling abl pre-B cells also exhibited induction of *Brca2*, *Palb2* and *Rad51,* which function to replace RPA with RAD51 on ssDNA to form RAD51 nucleofilaments at DSBs during HR (Figures 5C, 5D and S3). Indeed, there was a significant increase in the number of RAD51 foci in non-cycling *Lig4*$^{-/-}$*:Lin37*$^{-/-}$ abl-pre-B cells after IR as compared to *Lig4*$^{-/-}$ abl-pre-B cells (Figures 6B and S4). Once formed, a RAD51 nucleofilament will initiate a homology search and HR-mediated DSB repair (Prakash et al. 2015). Indeed, using the HPRT-DR-GFP reporter for DSB repair by HR, we observed an increase in homology-mediated DSB repair in non-cycling *Lig4*$^{-/-}$*:Lin37*$^{-/-}$ abl-pre-B cells as compared to *Lig4*$^{-/-}$ abl-pre-B cells (Figure 6C) (Pierce et al. 2001). We conclude that in the absence of LIN37, the extensive DNA end resection can lead to HR-mediated DSB repair in non-cycling cells. Moreover, this occurs in the presence of 53BP1.

LIN37 uniquely prevents DNA end resection in quiescent G_0 cells: We find that LIN37 is required to prevent DNA end resection and subsequent HR steps in non-cycling cells that have 2N DNA content and do not incorporate BrdU indicating that they are in G_0 or G_1. To distinguish between G_0 and G_1 we assayed non-cycling imatinib-treated abl pre-B cells and EGF-deprived MCF10A cells for expression of the cyclin dependent kinase, CDK4, and phospho-CDK4, which along with CDK6 is required for non-cycling quiescent G_0 cells to move into G_1 (Figures 7A and 7B) (Malumbres and Barbacid 2001, Pennycook and Barr 2020). Both non-cycling abl pre-B cells and MCF10A cells had low levels of CDK4 and phsopho-CDK4 indicative of them being in G_0 (Figures 7A and 7B). Rb suppresses genes encoding proteins required for G_0 cells to transit to G_1 and then into S-phase (Weinberg 1995, Pennycook and Barr 2020, Sadasivam and DeCaprio 2013). The phosphorylation of Rb by CDK4 or CDK6 leads to its inactivation and the transit of cells from G_0 to G_1 (Weinberg 1995, Pennycook and Barr 2020). Phospho-Rb was not detected by western blotting of imatinib-treated abl pre-B cells or MCF10A cells deprived of EGF indicating that these cells are in G_0 (Figures 7A and 7B). PCNA, which is expressed early in the transition from G_1 to S was also not detected in these cells (Figures 7A and 7B). Together these data indicate that imatinib treated abl pre-B cells and MCF10A cells deprived of EGF have exited the cell cycle and

373 entered G_0, also known as quiescence, and LIN37 is required to protect DNA
374 ends from resection in these cells.
375
376 Cycling cells in G_1-phase also rely on NHEJ to repair DNA DSBs and we next
377 asked whether LIN37 also functions to protect DNA ends from resection in
378 these cells. To this end we employed the PIP-FUCCI cell cycle sensor to isolate
379 G_1 and S/G_2/M populations from cycling *Lig4*$^{-/-}$, *Lig4*$^{-/-}$*:53bp1*$^{-/-}$ and *Lig4*$^{-/-}$*:Lin37*$^{-/-}$ abl pre-B cells and wild type, *53bp1*$^{-/-}$ and *Lin37*$^{-/-}$ MCF10A cells by flow
380
381 cytometric cell sorting (Grant et al. 2018). The effectiveness of this purification
382 was evidenced by the absence of Cyclin A in G_1-phase cells (Figures 7C and
383 7D) (Henglein et al. 1994). Western blot analysis revealed that in contrast to G_0
384 cells, G_1 cells expressed detectable levels of the HR proteins BRCA1, BARD1,
385 BLM, FANCD2 and RAD51. Moreover, loss of LIN37 did not lead to a significant
386 increase in the levels of these proteins in G_1-phase cells isolated from
387 proliferating populations (Figures 7C and 7D).
388
389 We next asked whether LIN37 functions to protect DNA ends from extensive
390 end resection in cycling G_1-phase cells. To do this, we incubated proliferating
391 *Lig4*$^{-/-}$, *Lig4*$^{-/-}$*:53bp1*$^{-/-}$ and *Lig4*$^{-/-}$*:Lin37*$^{-/-}$ abl pre-B cells and wild type, *53bp1*$^{-/-}$
392 and *Lin37*$^{-/-}$ MCF10A cells in media containing EdU, which was incorporated
393 into newly-synthesized DNA allowing for the detection of S-phase cells. After

IR, RPA association with DNA DSBs was assayed by flow cytometry in G_1-phase cells, which were identified as cells being EdU-negative and having 2N DNA content (Figures S5A and S5B). In contrast to G_0 cells, which are dependent on 53BP1 and Lin37 for DNA end protection, G_1 cells appear to depend primarily on 53BP1 as evidenced by the substantial increase in RPA association with chromatin in IR treated 53BP1-deficient G_1-phase cells as compared to LIN37-deficient G_1-phase cells (Figures 7E and 7F). We conclude that LIN37 functions to prevent DNA end resection primarily in quiescent G_0 cells while 53BP1 functions in both proliferating G_1 and quiescent G_0 phase cells.

Discussion

Rb and the DREAM complex are transcriptional repressors that silence the expression of genes required to promote cell cycle, driving cells to exit the cell cycle an enter G_0 or quiescence, where most cells in the human body reside (Mages et al. 2017, Weinberg 1995). Quiescent G_0 cells and cycling cells in G_1-phase have 2N DNA content and rely on NHEJ to repair DNA DSBs and maintain genome stability. 53BP1 and its downstream effectors are required to promote NHEJ in G_0 and G_1 cells by antagonizing DNA end resection and ssDNA generation (Mirman and de Lange 2020, Setiaputra and Durocher 2019). However, here we show that in G_0 cells, DNA end protection also requires LIN37, a component of the DREAM complex. Moreover, LIN37 function also prevents aberrant homology-mediated joining in G_0 cells.

LIN37 association with DREAM is required for its transcriptional repressor function, but is not required for the binding of the complex to its target genes (Mages et al. 2017). In addition to genes encoding proteins that promote cell cycle, DREAM complex binding sequences, termed cell cycle genes homology regions (CHRs), are also found in the promoter regions of many HR genes (Mages et al. 2017, Muller et al. 2014). Several lines of evidence presented here demonstrate that in G_0 cells LIN37 functions through DREAM transcriptional repression to protect DNA ends from resection. Loss of LIN37 in

G_0 cells leads to the expression of many HR genes that promote DNA end resection such as *Brca1*, *Bard1*, *Blm* and *Fancd2* (Figure 5B and Table S2). Moreover, this increased gene expression leads to a significant increase in the levels of these proteins in G_0 cells (Figures 5C, 5D and S3). Loss of BRCA1, BARD1, BLM or FANCD2 in LIN37-deficient G_0 cells prevents DNA end resection demonstrating that each of these function of each of these proteins is required to promote DNA end resection in these cells (Figure 6A). Finally, while the expression of wild type LIN37 in LIN37-deficient G_0 cells prevents the expression of HR genes and DNA end resection the expression of $LIN37^{CD}$, which cannot participate in forming a functional DREAM repressor complex, does not (Figure 5E).

LIN37-DREAM and 53BP1 function in distinct ways to protect DNA ends from aberrant resection. This notion is supported by the additive effect on resection in *Lig4*$^{-/-}$ G_0 abl pre-B cells lacking both 53BP1 and LIN37, as compared to those lacking 53BP1 or LIN37 in (Figures 4D and 4E). Resection in G_0 LIN37-deficienct cells relies on BRCA1, BARD1, BLM and FANCD2 as evidenced by the lack of DNA end resection in LIN37-deficienct cells that have lost expression of any of these proteins through bulk gene inactivation (Figure 6A). In contrast, 53BP1-deficienct G_0 cells express low levels of BRCA1, BARD1, BLM and FANCD2 and bulk inactivation of the genes encoding these proteins does not

impact DNA end resection in these cells (Figure 6A). Thus, in G_0 cells LIN37 prevents BRCA1-dependent DNA end resection whereas 53BP1 protects DNA ends from BRCA1-independent resection pathways.

Cycling cells in G_1-phase also must repair DSBs by NHEJ and thus need to protect DNA ends from excess resection. In contrast to what we observe in G_0 cells, the loss of LIN37 in cycling cells in G_1-phase does not lead to alterations in HR protein levels or aberrant resection of DNA ends as evidenced by increased RPA association at DSBs (Figure 7). In G_1-phase cells, 53BP1-RIF1 prevents BRCA1-CTIP from associating with DSBs and promoting resection (Escribano-Diaz et al. 2013, Chapman et al. 2013). In contrast, in S/G_2-phase cells this regulatory balance is tipped with BRCA1 inhibiting RIF1 association with DSBs, which would otherwise antagonize resection (Escribano-Diaz et al. 2013, Chapman et al. 2013). Like G_1-phase cells, in G_0 cells 53BP1 functions to protect DNA ends from resection. However, upon the loss of LIN37 in G_0 cells the expression of HR proteins, including BRCA1, does not inactivate the 53BP1 pathway. Indeed, we find robust 53BP1-RIF1 association with DSBs in LIN37-deficient G_0 cells and the loss of 53BP1 in these cells leads to increased RPA association at DSBs indicating that 53BP1 functions in DNA end protection in these cells (Figures 4B-E, S2B and S2C). We speculate that the genetic program activated by the loss of LIN37 in G_0 cells leads to the activation of

469 pathways that regulate the balance of anti-resection 53BP1 activities and pro-
470 resection BRCA1 activities in a manner that favors DNA end resection.
471 Although the identity of these pathways and the manner in which they function
472 is unknown, they do not prevent 53BP1-RIF1 association at DSBs in G_0 cells.
473
474 While LIN37-DREAM and 53BP1 both inhibit DNA end resection in G_0 cells,
475 LIN37-DREAM has additional activities in promoting genome stability by
476 preventing resected DNA ends from progressing in HR-mediated DSB repair.
477 LIN37-deficient G_0 cells express BRCA2, PALB2 and RAD51 that convert RPA-
478 coated ssDNA at broken DNA ends to RAD51 nucleofilaments that can mediate
479 homology mediated repair (Figures 5B-D, 6B, 6C, S3, S4 and Table S2), which
480 in G_0 cells could lead to aberrant homology-mediated DNA end joining and
481 chromosomal aberrations such as deletions and translocations. Thus, in
482 quiescent cells in the body, LIN37-DREAM promotes genome stability by both
483 antagonizing DNA end resection and preventing the aberrantly homology-
484 mediated joining of resected DNA ends.
485

Figure 1

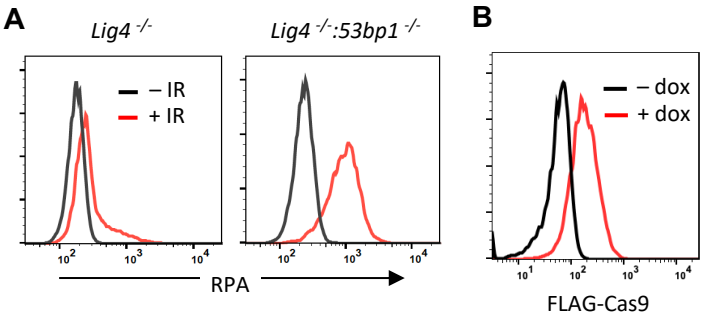

D

Gene	Enrichment score	Gene	Enrichment score
53bp1	4, 2, 2, 2, 2	*Ctc1*	4, 3, 3, 2, 1
Rif1	4, 4, 3, 2, 1	*Stn1*	5, 5, 4, 4, 2
Shld1	2, 2, 2, 1, 1	*Ten1*	3, 3, 3, 1, 1
Shld2	3, 2, 2, 2, 2	*Lin37*	5, 5, 5, 2, 1

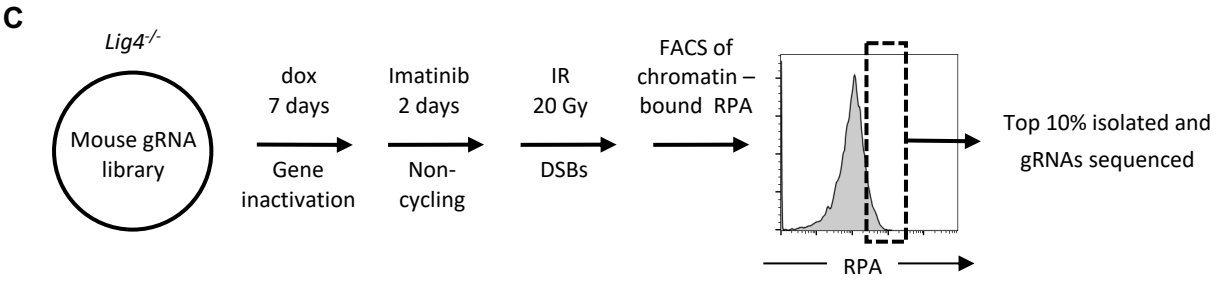

Figure 1. An unbiased genome-scale gRNA screen for novel DNA end protection factors

(A) Flow cytometric analysis of chromatin-bound RPA before and after IR of non-cycling *Lig4*$^{-/-}$ and *Lig4*$^{-/-}$:*53bp1*$^{-/-}$ abl pre-B cells. (B) Flow cytometric analysis of FLAG-Cas9 in *Lig4*$^{-/-}$ cells with (+dox) and without (-dox) doxycycline to induce expression of FLAG-Cas9. (C) Schematic diagram of the genome-scale guide RNA screen for genes preventing DNA end resection in non-cycling *Lig4*$^{-/-}$ abl pre-B cells. (D) Enrichment score (fold enrichment) of individual gRNAs to a subset of genes identified in the RPA high population.

Figure 2

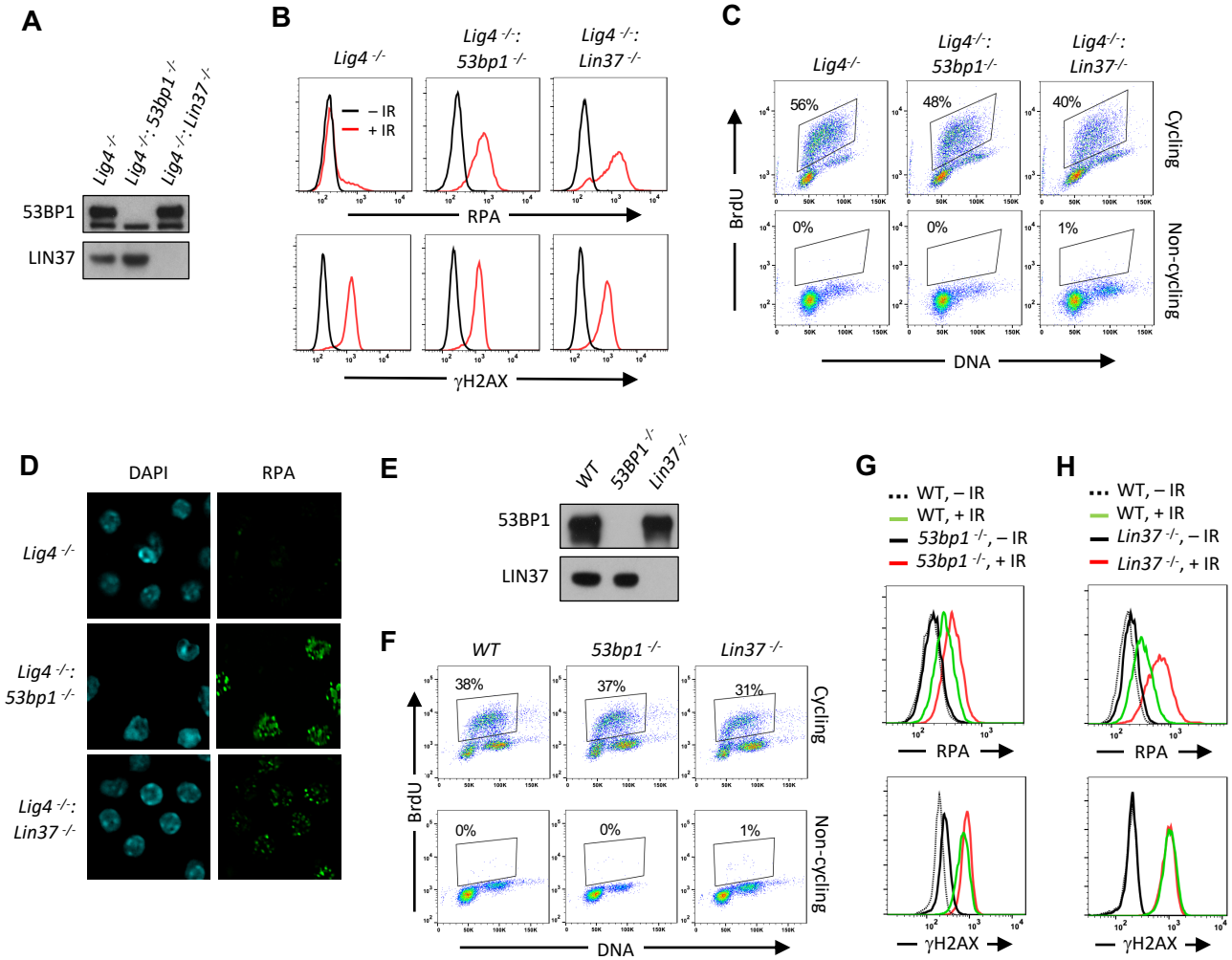
A
Lig4 -/-
Lig4 -/-: 53bp1 -/-
Lig4 -/-: Lin37 -/-
53BP1
LIN37
B
Lig4 -/-
Lig4 -/-: 53bp1 -/-
Lig4 -/-: Lin37 -/-
– IR
+ IR
RPA
γH2AX
C
Lig4-/-
Lig4-/-: 53bp1-/-
Lig4-/-: Lin37-/-
56%
48%
40%
0%
0%
1%
Cycling
Non-cycling
BrdU
DNA
D
DAPI
RPA
Lig4 -/-
Lig4 -/-: 53bp1 -/-
Lig4 -/-: Lin37 -/-
E
WT
53BP1 -/-
Lin37 -/-
53BP1
LIN37
F
WT
53bp1 -/-
Lin37 -/-
38%
37%
31%
0%
0%
1%
Cycling
Non-cycling
BrdU
DNA
G
WT, – IR
WT, + IR
53bp1 -/-, – IR
53bp1 -/-, + IR
RPA
γH2AX
H
WT, – IR
WT, + IR
Lin37 -/-, – IR
Lin37 -/-, + IR
RPA
γH2AX

Figure 2. Non-cycling LIN37-deficient cells accumulate chromatin-bound RPA after IR-induced damage

(A) Western blot of indicated proteins in *Lig4*$^{-/-}$, *Lig4*$^{-/-}$:*53bp1*$^{-/-}$ and *Lig4*$^{-/-}$:*Lin37*$^{-/-}$ abl pre-B cells. (B) Flow cytometric analysis of chromatin-bound RPA (top) and γH2AX (bottom) before and after IR of non-cycling *Lig4*$^{-/-}$, *Lig4*$^{-/-}$:*53bp1*$^{-/-}$ and *Lig4*$^{-/-}$:*Lin37*$^{-/-}$ abl pre-B cells. The experiments were repeated in two independently generated cell lines at least twice. (C) Flow cytometric analysis of cycling and non-cycling *Lig4*$^{-/-}$, *Lig4*$^{-/-}$:*53bp1*$^{-/-}$ and *Lig4*$^{-/-}$:*Lin37*$^{-/-}$ abl pre-B cells for BrdU incorporation and DNA content (7-AAD). Percentage of cells in S-phase is indicated. (D) Representative images of IR-induced RPA foci in non-cycling *Lig4*$^{-/-}$, *Lig4*$^{-/-}$:*53bp1*$^{-/-}$ and *Lig4*$^{-/-}$:*Lin37*$^{-/-}$ abl pre-B cells from two independent experiments. (E) Western blot analysis of indicated proteins in *WT*, *53bp1*$^{-/-}$ and *Lin37*$^{-/-}$ MCF10A cells. (F) Flow cytometric analysis of BrdU pulsed cycling (top) or non-cycling (bottom) *WT*, *53bp1*$^{-/-}$ and *Lin37*$^{-/-}$ MCF10A cells as in (C). (G, H) Flow cytometric analysis of chromatin-bound RPA (top) and γH2AX (bottom) before or after IR of non-cycling *WT* and (G) *53bp1*$^{-/-}$ or (H) *Lin37*$^{-/-}$ MCF10A cells.

Figure 3

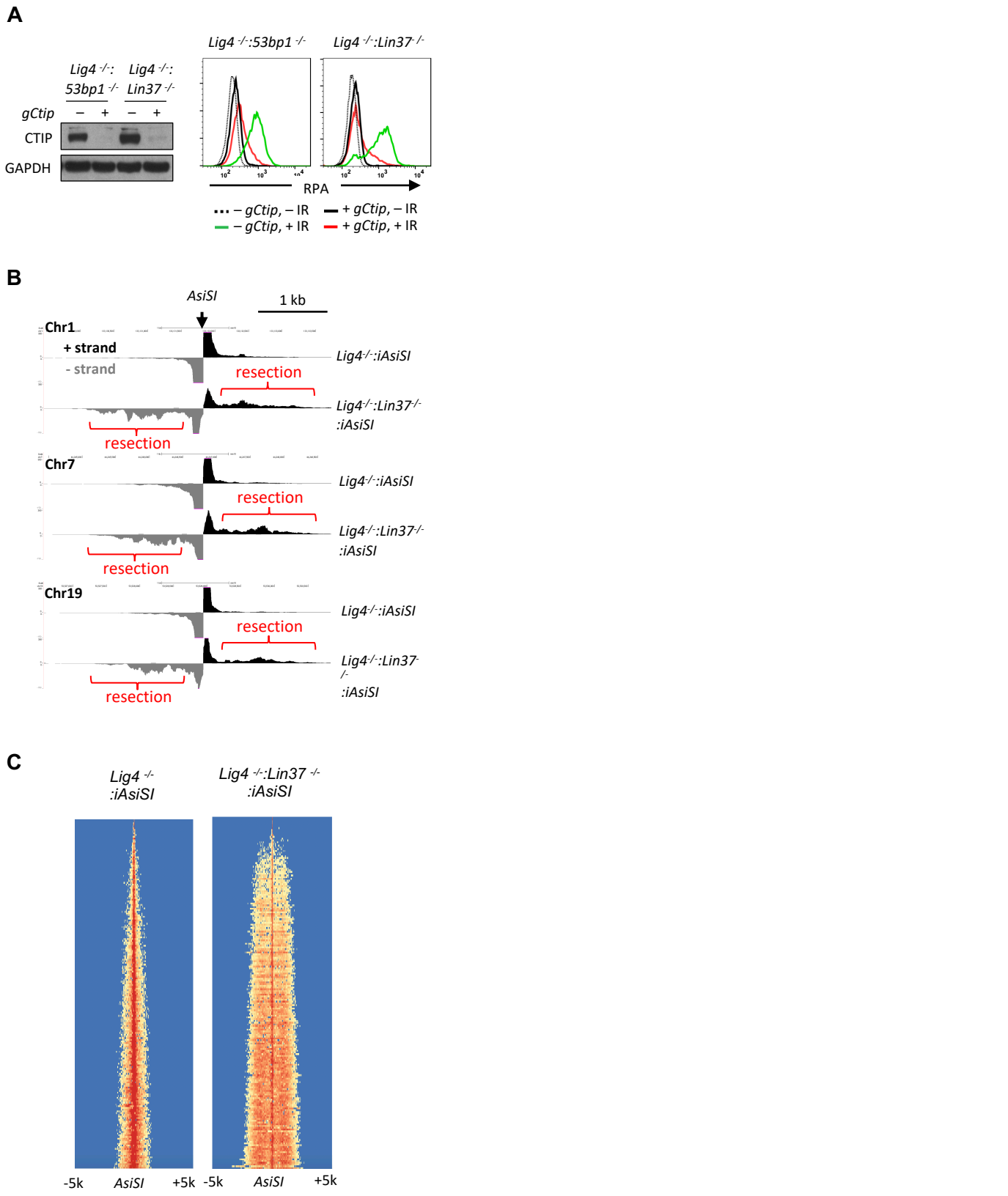
A
Lig4 -/-:53bp1 -/-
Lig4 -/-:Lin37 -/-
Lig4 -/-: 53bp1 -/-
Lig4 -/-: Lin37 -/-
gCtip
– + – +
CTIP
GAPDH
RPA
– gCtip, – IR
+ gCtip, – IR
– gCtip, + IR
+ gCtip, + IR
B
AsiSI
1 kb
Chr1
+ strand
- strand
resection
Lig4-/-:iAsiSI
Lig4-/-:Lin37-/-:iAsiSI
Chr7
Chr19
C
Lig4 -/-:iAsiSI
Lig4 -/-:Lin37 -/-:iAsiSI
-5k
AsiSI
+5k

Figure 3. LIN37 prevents DNA end resection in non-cycling cells

(A) Cas9-induced *Lig4*$^{-/-}$:*53bp1*$^{-/-}$ and *Lig4*$^{-/-}$:*Lin37*$^{-/-}$ abl pre-B cells with (+) and without (-) the *Ctip* gRNA (*gCtip*). Western blot with indicated antibodies (left) and flow cytometric analysis of chromatin-bound RPA before and after IR of the non-cycling cells (right) are shown. Representative of three experiments. (B) End-seq tracks of representative *AsiSI* sites on mouse chromosomes 1, 7 and 19 in non-cycling *Lig4*$^{-/-}$ and *Lig4*$^{-/-}$:*Lin37*$^{-/-}$ abl pre-B cells. (C) The heatmaps of End-seq at *AsiSI* DSBs across the mouse genome (y axis) after *AsiSI* induction in non-cycling *Lig4*$^{-/-}$ and *Lig4*$^{-/-}$:*Lin37*$^{-/-}$ abl pre-B cells. Two experiments were carried out in two independently generated *Lig4*$^{-/-}$:*iAsiSI* and *Lig4*$^{-/-}$:*Lin37*$^{-/-}$:*iAsiSI* clones.

Figure 4

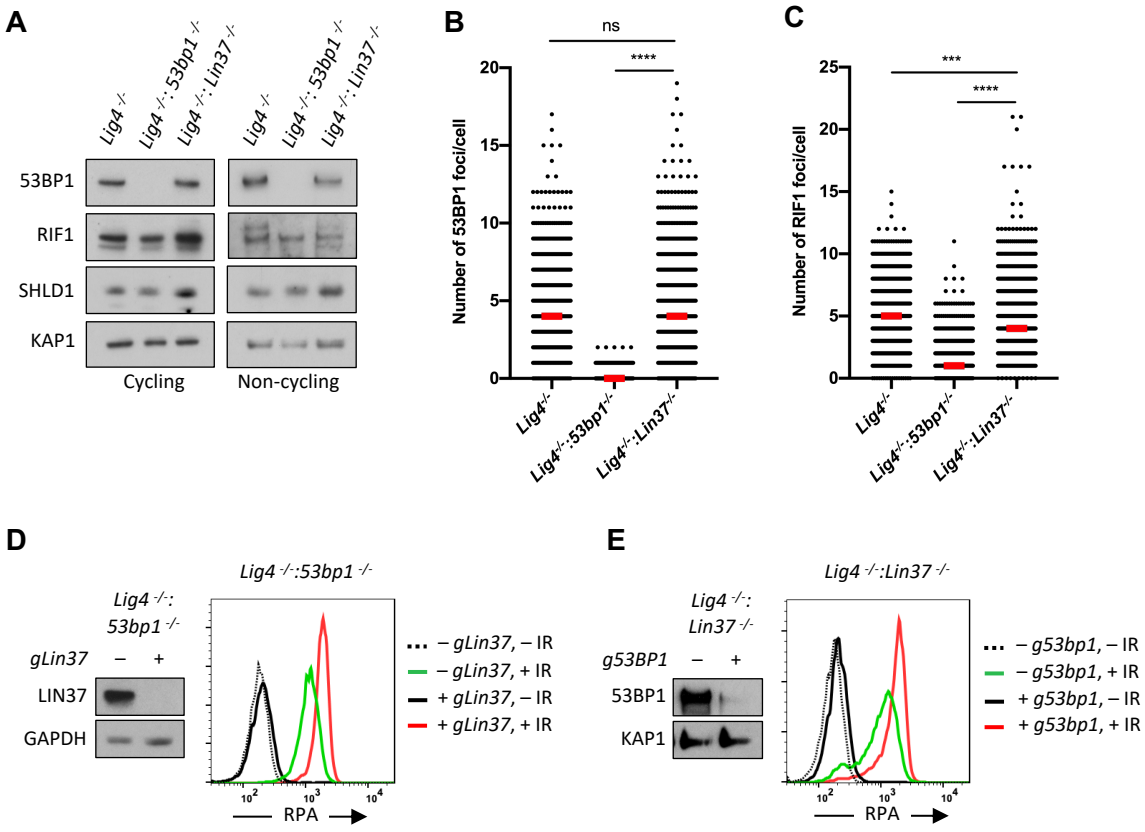
A
Lig4 -/-
Lig4 -/-:53bp1 -/-
Lig4 -/-:Lin37 -/-
Lig4 -/-
Lig4 -/-:53bp1 -/-
Lig4 -/-:Lin37 -/-
53BP1
RIF1
SHLD1
KAP1
Cycling
Non-cycling
B
ns
****
Number of 53BP1 foci/cell
20
15
10
5
0
Lig4-/-
Lig4-/-:53bp1-/-
Lig4-/-:Lin37-/-
C
***
****
Number of RIF1 foci/cell
25
20
15
10
5
0
Lig4-/-
Lig4-/-:53bp1-/-
Lig4-/-:Lin37-/-
D
Lig4 -/-:53bp1 -/-
Lig4 -/-:
53bp1 -/-
gLin37 – +
LIN37
GAPDH
– gLin37, – IR
– gLin37, + IR
+ gLin37, – IR
+ gLin37, + IR
RPA
E
Lig4 -/-:Lin37 -/-
Lig4 -/-:
Lin37 -/-
g53BP1 – +
53BP1
KAP1
– g53bp1, – IR
– g53bp1, + IR
+ g53bp1, – IR
+ g53bp1, + IR
RPA

Figure 4. 53BP1 and LIN37 have distinct DNA end protection functions

(A) Western blot of indicted proteins in cycling and non-cycling *Lig4*$^{-/-}$, *Lig4*$^{-/-}$:*53bp1*$^{-/-}$ and *Lig4*$^{-/-}$:*Lin37*$^{-/-}$ abl pre-B cells. (B, C) Quantification of 53BP1 (B) or RIF1 (C) foci after IR treatment of non-cycling *Lig4*$^{-/-}$, *Lig4*$^{-/-}$:*53bp1*$^{-/-}$ and *Lig4*$^{-/-}$:*Lin37*$^{-/-}$ abl pre-B cells. Red bars indicate the median number of foci in each sample. More than 1000 cells were analyzed in each cell line in two independent experiments (****p<0.0001, ***p=0.0002, Mann-Whitney test). (D, E) Flow cytometric analysis of chromatin-bound RPA before and after IR of non-cycling *Lig4*$^{-/-}$:*53bp1*$^{-/-}$(D) or *Lig4*$^{-/-}$:*Lin37*$^{-/-}$ (E) abl pre-B cells after bulk gene inactivation of *Lin37* (*gLin37*) or *53bp1* (*g53bp1*), respectively. Representative of three experiments.

Figure 5

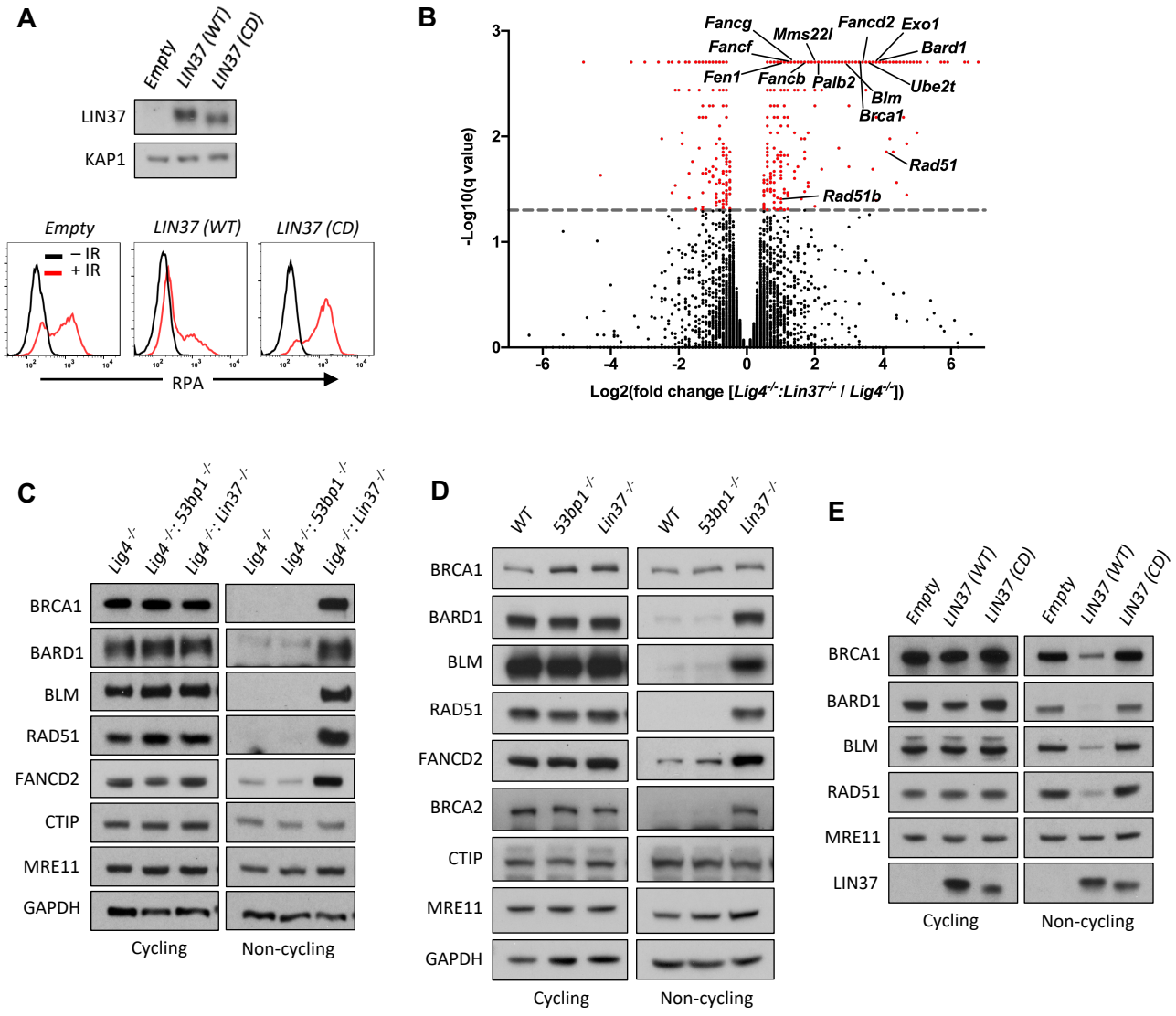
A
Empty
LIN37 (WT)
LIN37 (CD)
LIN37
KAP1
Empty
LIN37 (WT)
LIN37 (CD)
– IR
+ IR
RPA
B
Fancg
Mms22l
Fancd2
Exo1
Fancf
Bard1
Fen1
Fancb
Palb2
Ube2t
Blm
Brca1
Rad51
Rad51b
-Log10(q value)
Log2(fold change [Lig4-/-:Lin37-/- / Lig4-/-])
C
Lig4-/-
Lig4-/-: 53bp1-/-
Lig4-/-: Lin37-/-
BRCA1
BARD1
BLM
RAD51
FANCD2
CTIP
MRE11
GAPDH
Cycling
Non-cycling
D
WT
53bp1-/-
Lin37-/-
BRCA1
BARD1
BLM
RAD51
FANCD2
BRCA2
CTIP
MRE11
GAPDH
Cycling
Non-cycling
E
Empty
LIN37 (WT)
LIN37 (CD)
BRCA1
BARD1
BLM
RAD51
MRE11
LIN37
Cycling
Non-cycling

Figure 5. LIN37 suppresses the expression of HR protein expression in non-cycling cells

(A) Western blot (top) and flow cytometric analysis for chromatin bound RPA after before or after IR (bottom) of non-cycling *Lig4*$^{-/-}$:*Lin37*$^{-/-}$ abl pre-B cells with empty lentivirus or lentivirus expressing wild type (WT) LIN37 or the LIN37 (CD) mutant. Representative of three experiments. (B) Volcano plot of RNA seq analysis of non-cycling *Lig4*$^{-/-}$ and *Lig4*$^{-/-}$:*Lin37*$^{-/-}$ abl pre-B cells showing log2 values of the ratio of normalized transcript levels of *Lig4*$^{-/-}$: *Lin37*$^{-/-}$ to *Lig4*$^{-/-}$ cells (X-axis) and -log10 of the q-values of fold enrichment of each gene (Y-axis). The dash line indicates q = 0.05. Genes with q values ≤ 0.05 are denoted as red dots. (C) Western blot of indicated proteins in cycling and non-cycling *Lig4*$^{-/-}$, *Lig4*$^{-/-}$:*53bp1*$^{-/-}$ and *Lig4*$^{-/-}$:*Lin37*$^{-/-}$ abl pre-B cells. (D) Western blot analysis of indicated proteins in cycling or non-cycling *WT,* *53bp1*$^{-/-}$ and *Lin37*$^{-/-}$ MCF10A cells. (E) Western blot of indicated proteins in cycling and non-cycling *Lig4*$^{-/-}$:*Lin37*$^{-/-}$ abl pre-B cells with empty lentivirus or lentivirus expressing wild type (WT) LIN37 or the LIN37 (CD) mutant.

Figure 6

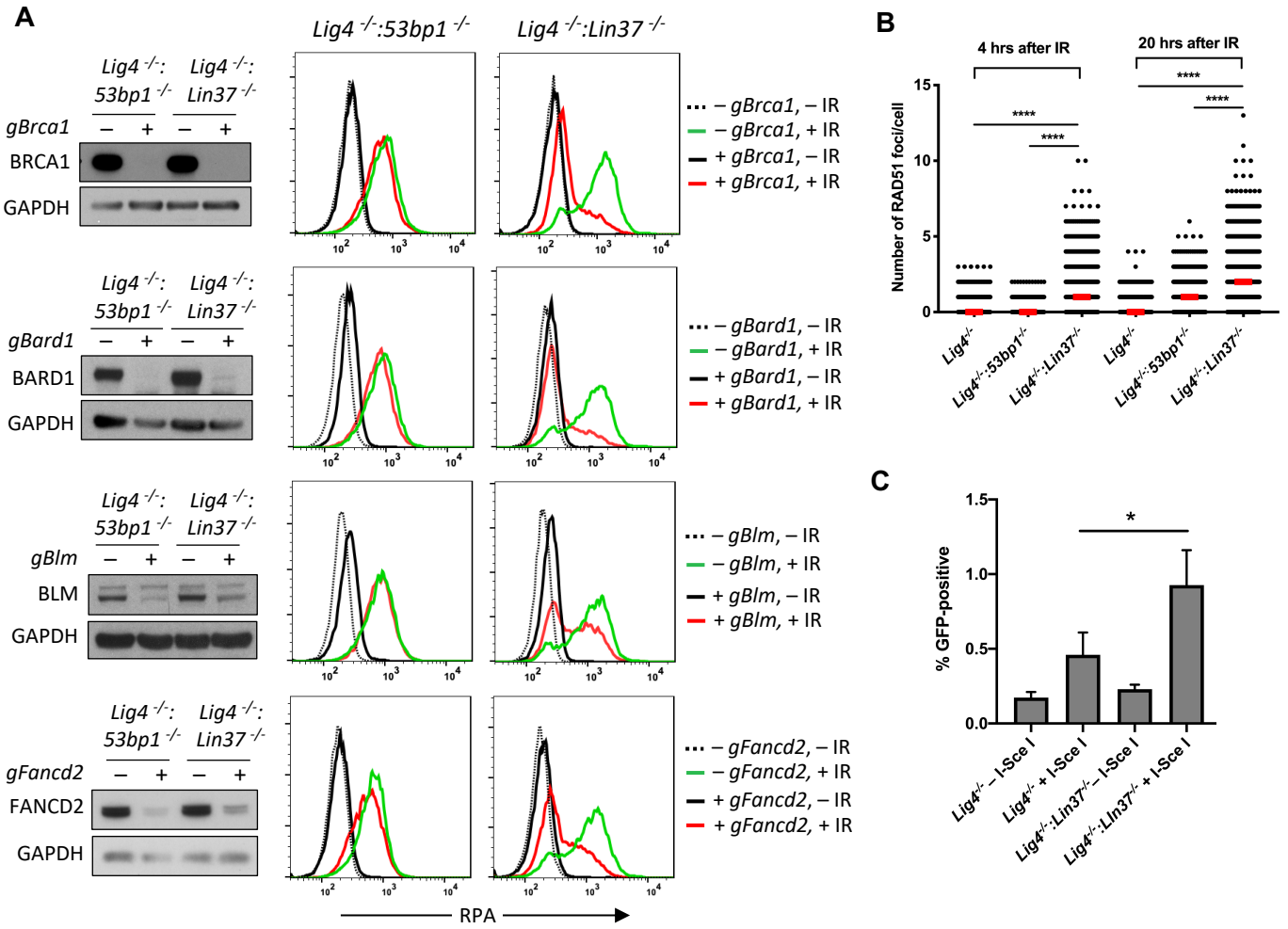
A
Lig4 -/-:53bp1 -/-
Lig4 -/-:Lin37 -/-
gBrca1
BRCA1
GAPDH
gBard1
BARD1
GAPDH
gBlm
BLM
GAPDH
gFancd2
FANCD2
GAPDH
– gBrca1, – IR
– gBrca1, + IR
+ gBrca1, – IR
+ gBrca1, + IR
– gBard1, – IR
– gBard1, + IR
+ gBard1, – IR
+ gBard1, + IR
– gBlm, – IR
– gBlm, + IR
+ gBlm, – IR
+ gBlm, + IR
– gFancd2, – IR
– gFancd2, + IR
+ gFancd2, – IR
+ gFancd2, + IR
RPA
B
4 hrs after IR
20 hrs after IR
Number of RAD51 foci/cell
****
C
% GFP-positive
*
I-Sce I

Figure 6. LIN37 Prevents resection and HR through suppressing HR protein expression in non-cycling cells

(A) Flow cytometric analysis of chromatin-bound RPA before and after IR of non-cycling *Lig4*$^{-/-}$:*53bp1*$^{-/-}$ or *Lig4*$^{-/-}$:*Lin37*$^{-/-}$ abl pre-B cells with or without indicated gRNAs following Cas9 induction for bulk gene inactivation. Representative experiments of three. (B) Quantification of RAD51 foci in non-cycling *Lig4*$^{-/-}$, *Lig4*$^{-/-}$:*53bp1*$^{-/-}$ and *Lig4*$^{-/-}$:*Lin37*$^{-/-}$ abl pre-B cells 4 and 20 hours after IR. Red bars indicate the median number of RAD51 foci in each sample of more than 1000 cells analyzed for each cell line. Representative of two independent experiments (****p<0.0001, Mann-Whitney test). (C) Flow cytometric analysis of HR-mediated DSB repair in non-cycling *Lig4*$^{-/-}$ and *Lig4*$^{-/-}$:*Lin37*$^{-/-}$ abl pre-B cells using the HPRT-DR-GFP reporter. The percentage of GFP-positive cells is shown. Error bars are ± SEM from 3 experiments (*p=0.0124, t-test).

Figure 7

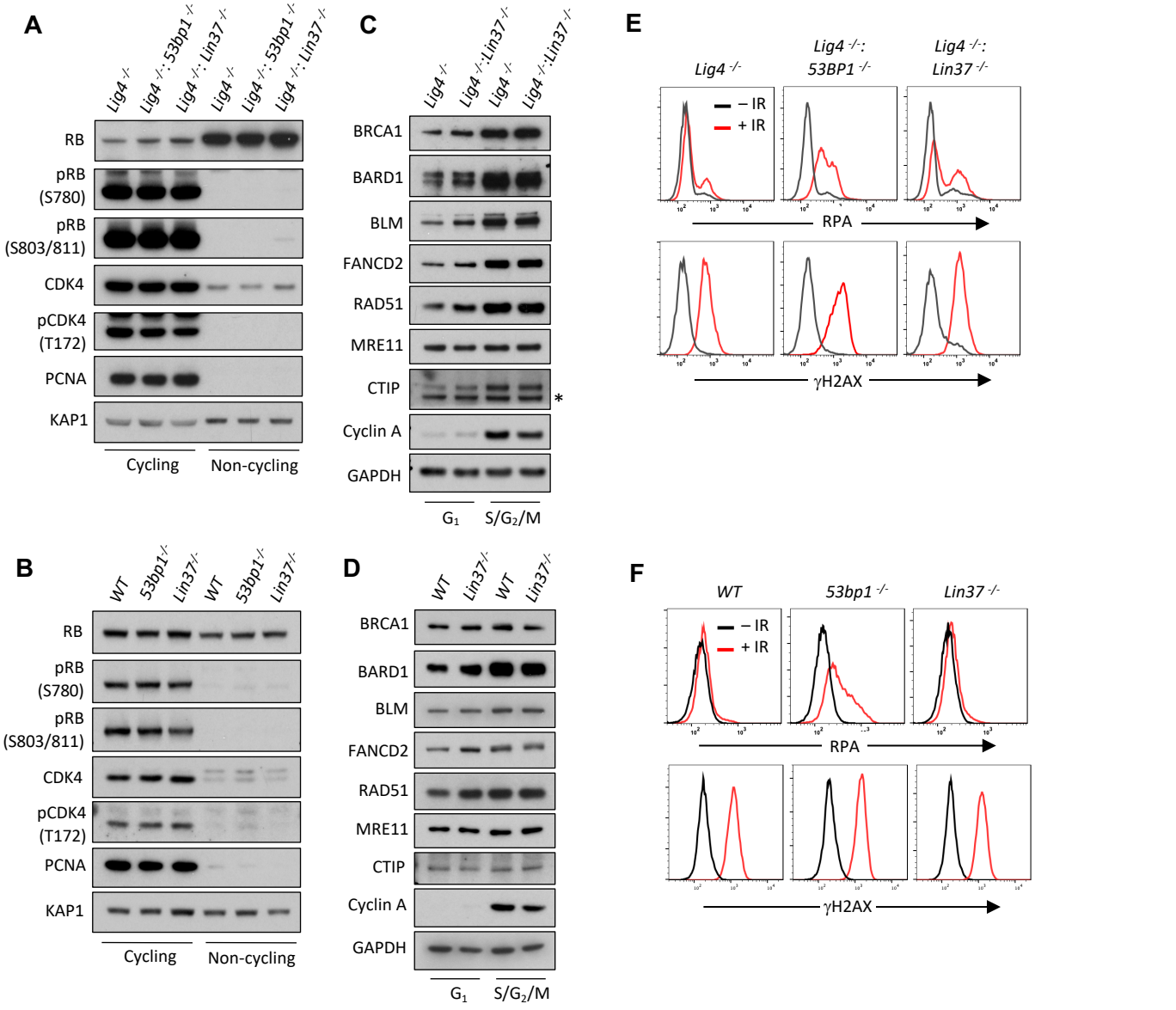
A
Lig4 -/-
Lig4 -/-: 53bp1 -/-
Lig4 -/-: Lin37 -/-
Lig4 -/-
Lig4 -/-: 53bp1 -/-
Lig4 -/-: Lin37 -/-
RB
pRB (S780)
pRB (S803/811)
CDK4
pCDK4 (T172)
PCNA
KAP1
Cycling
Non-cycling
C
Lig4 -/-
Lig4 -/-:Lin37 -/-
Lig4 -/-
Lig4 -/-:Lin37 -/-
BRCA1
BARD1
BLM
FANCD2
RAD51
MRE11
CTIP
*
Cyclin A
GAPDH
G1
S/G2/M
E
Lig4 -/-
Lig4 -/-: 53BP1 -/-
Lig4 -/-: Lin37 -/-
– IR
+ IR
RPA
γH2AX
B
WT
53bp1 -/-
Lin37 -/-
WT
53bp1 -/-
Lin37 -/-
RB
pRB (S780)
pRB (S803/811)
CDK4
pCDK4 (T172)
PCNA
KAP1
Cycling
Non-cycling
D
WT
Lin37 -/-
WT
Lin37 -/-
BRCA1
BARD1
BLM
FANCD2
RAD51
MRE11
CTIP
Cyclin A
GAPDH
G1
S/G2/M
F
WT
53bp1 -/-
Lin37 -/-
– IR
+ IR
RPA
γH2AX

Figure 7. LIN37 function in DNA end protection is restricted to G_0

(A, B) Western blot of indicated proteins in cycling and non-cycling abl pre-B cells (A) or MCF10A cells (B). (C, D) Western blot of indicated proteins in cycling G_1 or $S/G_2/M$ abl pre-B cells (C) or MCF10A cells (D), isolated by flow cytometric cell sorting based on the PIP-FUCCI reporter. Representative of two independent experiments. Asterisk indicates non-specific recognizing bands. (E, F) Flow cytometric analysis of chromatin bound RPA and γH2AX before and after IR treatment of G_1 phase *Lig4*$^{-/-}$, *Lig4*$^{-/-}$*:53bp1*$^{-/-}$ and *Lig4*$^{-/-}$*:Lin37*$^{-/-}$ abl pre-B cells (E) or *WT*, *53bp1*$^{-/-}$ and *Lin37*$^{-/-}$ MCF10A cells (F). Representative of three experiments.

Figure S1

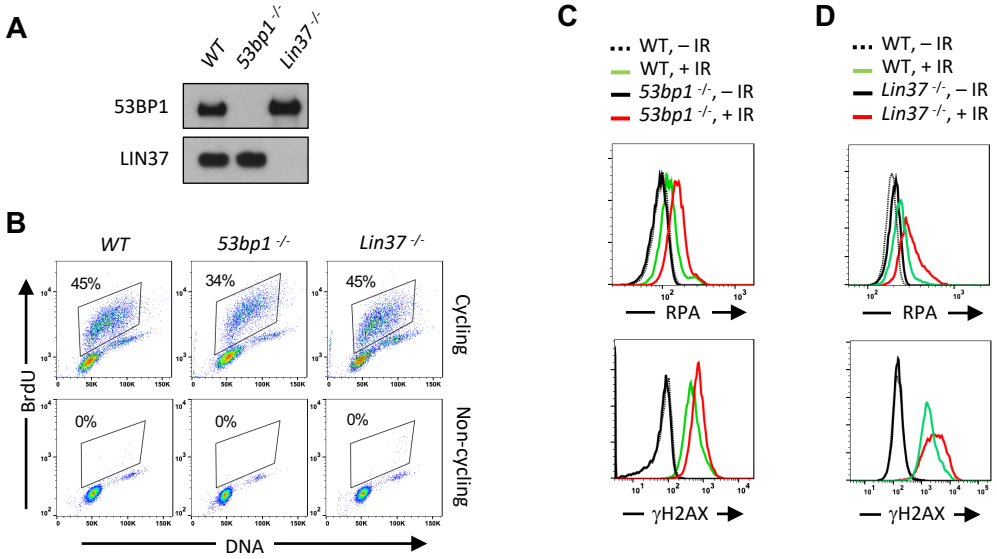
A
WT
53bp1 -/-
Lin37 -/-
53BP1
LIN37
B
WT
53bp1 -/-
Lin37 -/-
45%
34%
45%
0%
0%
0%
Cycling
Non-cycling
BrdU
DNA
C
WT, – IR
WT, + IR
53bp1 -/-, – IR
53bp1 -/-, + IR
RPA
γH2AX
D
WT, – IR
WT, + IR
Lin37 -/-, – IR
Lin37 -/-, + IR
RPA
γH2AX

Figure S1. Non-cycling LIN37-deficient cells accumulate chromatin-bound RPA after IR-induced damage

(A) Western blot analysis of indicated proteins in *WT*, *53bp1*$^{-/-}$ and *Lin37*$^{-/-}$ abl pre-B cells. (B) Flow cytometric analysis or BrdU and DNA (7AAD) of BrdU pulsed cycling (top) or non-cycling (bottom) *WT*, *53bp1*$^{-/-}$ and *Lin37*$^{-/-}$ abl pre-B cells. Percentage of cells in S-phase is indicated. (C, D) Flow cytometric analysis of chromatin-bound RPA (top panels) and γH2AX (bottom panels) before or after IR of non-cycling *WT* and *53bp1*$^{-/-}$ (C) or *Lin37*$^{-/-}$ (D) abl pre-B cells. The experiments were repeated in two independently generated cell lines at least twice.

Figure S2

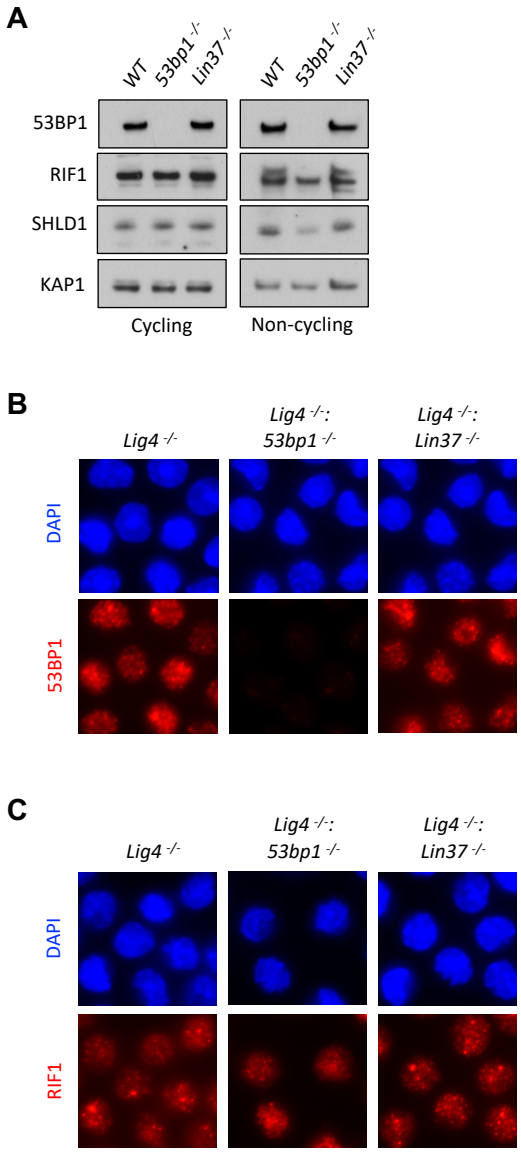
A
WT
53bp1 -/-
Lin37 -/-
WT
53bp1 -/-
Lin37 -/-
53BP1
RIF1
SHLD1
KAP1
Cycling
Non-cycling
B
Lig4 -/-
Lig4 -/-: 53bp1 -/-
Lig4 -/-: Lin37 -/-
DAPI
53BP1
C
Lig4 -/-
Lig4 -/-: 53bp1 -/-
Lig4 -/-: Lin37 -/-
DAPI
RIF1

Figure S2. 53BP1 and LIN37 have distinct DNA end protection functions

(A) Western blot of indicted proteins in cycling and non-cycling *WT*, *53bp1*$^{-/-}$ and *Lin37*$^{-/-}$ abl pre-B cells. (B, C) Representative images of 53BP1 (B) or RIF1 (C) foci after IR treatment of non-cycling *Lig4*$^{-/-}$, *Lig4*$^{-/-}$:*53bp1*$^{-/-}$ and *Lig4*$^{-/-}$:*Lin37*$^{-/-}$ abl pre-B cells.

Figure S3

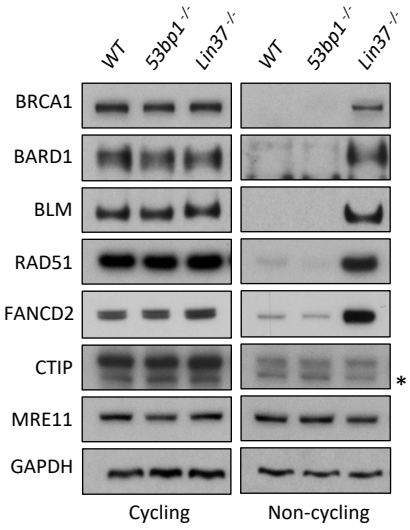
WT
53bp1-/-
Lin37-/-
WT
53bp1-/-
Lin37-/-
BRCA1
BARD1
BLM
RAD51
FANCD2
CTIP
*
MRE11
GAPDH
Cycling
Non-cycling

Figure S3. LIN37 suppresses HR protein expression in non-cycling cells

Western blot analysis of indicated proteins in cycling or non-cycling *WT,* *53bp1*$^{-/-}$ and *Lin37*$^{-/-}$ abl pre-B cells. * indicates non-specific bands.

Figure S4

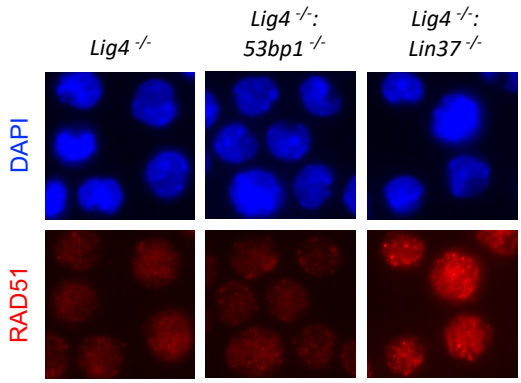

Figure S4. LIN37 deficiency leads to RAD51 focus formation in non-cycling abl pre-B cells

Representative images of RAD51 IR-induced foci in non-cycling *Lig4*$^{-/-}$, *Lig4*$^{-/-}$:*53bp1*$^{-/-}$ and *Lig4*$^{-/-}$:*Lin37*$^{-/-}$ abl pre-B cells.

Figure S5

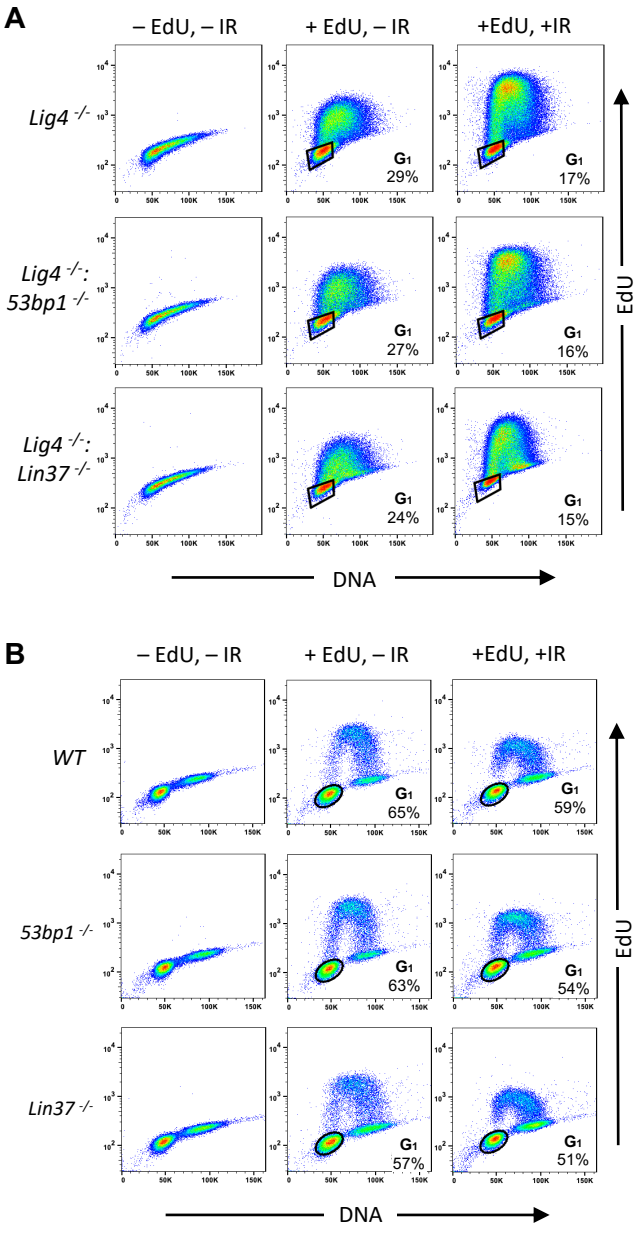
A
– EdU, – IR
+ EdU, – IR
+EdU, +IR
Lig4 -/-
Lig4 -/-: 53bp1 -/-
Lig4 -/-: Lin37 -/-
G1 29%
G1 17%
G1 27%
G1 16%
G1 24%
G1 15%
EdU
DNA
B
– EdU, – IR
+ EdU, – IR
+EdU, +IR
WT
53bp1 -/-
Lin37 -/-
G1 65%
G1 59%
G1 63%
G1 54%
G1 57%
G1 51%
EdU
DNA

Figure S5. Identification of G_1 phase cells in proliferating cells

(A, B) Flow cytometric analysis of EdU content and DNA (7AAD) of cycling *Lig4*$^{-/-}$, *Lig4*$^{-/-}$*:53bp1*$^{-/-}$ and *Lig4*$^{-/-}$*:Lin37*$^{-/-}$ abl pre-B cells (A) or cycling *WT*, *53bp1*$^{-/-}$ and *Lin37*$^{-/-}$ MCF10A cells (B). Cells were treated (+EdU) or not treated (-EdU) with EdU and analyses were carried out before or after IR. The percentage of G_1 phase cells is shown.

Acknowledgement: B.P.S. is supported by National Institutes of Health grants R01 AI047829 and R01 AI074953. J.K.T. is supported by National Institutes of Health grants R01 CA095641 and R01 GM064475.

Author Contributions: B.C., A.N, J.K.T and B.P.S. designed the study. and B.C. conducted all the experiments, except the ones specified below. Y.W. assisted genome-scale guide RNA CRISPR/Cas9 screen and performed data analysis. D.Z and F.F. performed imaging experiments. A.T.T., N.Z. and W.W. conducted End Seq and performed data analysis. A.B., C.C. and W.F. performed additional experiments. B.C., J.K.T and B.P.S wrote the manuscript with the help of A.N. All authors reviewed the manuscript.

Competing Interests: The authors declare no competing interests.

Materials and Methods

Cell lines and cell culture: Abelson virus-transformed pre-B cells (abl pre-B cells) were generated as described previously(Bredemeyer et al. 2006). DNA Ligase 4-deficient (*Lig4*$^{-/-}$) abl pre-B cells were generated by deleting the LoxP site-flanked *Lig4* coding sequence by expressing Cre recombinase(Helmink et al. 2011). WT and *Lig4*$^{-/-}$ abl pre-B cells and MCF10A human mammary epithelial cells used in this study all contain pCW-Cas9 (Addgene# 50661), which has a FLAG-tagged *Cas9* cDNA under the control of a doxycycline-inducible promoter. Intracellular staining with anti-FLAG and flow cytometry were used to identify clones homogeneously expressing FLAG-CAS9 after doxycycline treatment.

53bp1$^{-/-}$, *Lin37*$^{-/-}$, *Lig4*$^{-/-}$:*53bp1*$^{-/-}$ and *Lig4*$^{-/-}$:*53bp1*$^{-/-}$ cell lines were made by transiently transfecting *53bp1* or *Lin37* guide RNAs (gRNAs) in the pX330 vector (Addgene# 42230) into *WT* or *Lig4*$^{-/-}$ cells followed by subcloning by limited dilution. Knockout clones were verified by western blotting for loss of expression of the proteins encoded by genes targeted by the gRNAs. Abl pre-B cells were cultured in Dulbecco's Modified Eagle Medium (DMEM) supplemented with 10% fetal bovine serum (FBS) and 0.4% beta-mercaptoethanol, 100 U/ml penicillin/streptomycin, 1mM sodium pyruvate, 2mM L-glutamine,1X nonessential amino acids. MCF10A cells were cultured in

663 DMEM/F12 supplemented with 5% horse serum, 20ng/ml EGF, 0.5μg/ml
664 hydrocortisone, 100ng/ml cholera toxin, 10μg/ml insulin and 100U/ml penicillin-
665 streptomycin.
666
667 To render cells non-cycling, abl pre-B cells were treated with 3 μM imatinib
668 (Selleck Chemicals, S2475) for 2 (for chromatin-bound RPA assay) or 3 (for
669 gene expression analysis) days and MCF10A cells were grown in EGF-free
670 media for 2 days. At least two independent knockout clones of each gene in
671 each cell type were generated and used in the experiments in this study.
672 Knockout clones were verified by western blot for lack of expression of the
673 targeted proteins.
674
675 **Chromatin-bound RPA assay:** The chromatin-bound RPA flow cytometry
676 assay was carried out as described previously with modifications(Forment,
677 Walker, and Jackson 2012). Briefly, cells were washed with FACS wash (2%
678 FBS in 1X PBS) followed by pre-extraction in Triton X-100 on ice for 10 minutes
679 (0.05% for imatinib-treated abl pre-B cells, 0.2% for proliferating abl pre-B cells
680 and 0.5% for MCF10A cells). Cells were washed again with FACS wash and
681 fixed in BD Cytofix/Cytoperm at room temperature for 10 minutes. After fixation,
682 cells were incubated with anti-RPA32 antibody (Cell Signaling Technology,
683 2208S, 1:500) and anti-phospho-H2AX (S139) (Millipore Sigma, 05-636,

1:1000) in 1X BD Perm/Wash buffer at room temperature for 2 hours, followed by staining with Alexa Fluor 488 Goat anti-rat IgG (BioLegend, 405418, 1:500) and Alexa Fluro 647 Goat anti-moue IgG (BioLegend, 405322, 1:500) at room temperature for 1 hour. 20 μl of 7-AAD (BD Pharmingen, 559925) was added to each sample before resuspending cells in 300 μl of 1X PBS. RPA32 and phospho-H2AX(S139) levels were analyzed on a BD LSRFortessa Flow Cytometer.

For analysis of G_1 cells in a proliferating population, cells were pulsed with 10 μM EdU for 1 hour prior to irradiation. Irradiated cells were kept in EdU-containing media during the course of the experiments and processed as described above. Following RPA32 and phosphor-H2AX(S139), click-IT chemistry was performed as per manufacturer's instructions.

Non-cycling abl pre-B cells were exposed to 15 Gy of IR and analyzed 18 hours after irradiation. Cycling abl pre-B cells were analyzed 3 hours after 5 Gy of IR. Non-cycling MCF10A were exposed to 30 Gy of IR and analyzed 4 hours after irradiation. Cycling MCF10A cells were analyzed 6 hours after 25 Gy IR.

Genome-wide guide RNA CRISPR/Cas9 screen: *Lig4*$^{-/-}$ or *Lig4*$^{-/-}$*:Lin37*$^{-/-}$ abl pre-B cells were transduced with lentiviral mouse genome-wide CRISPR gRNA

library V2 (Addgene #67988) by centrifuging a cell and viral supernatant mixture (supplemented with 5μg/ml polybrene) at 1,800 rpm for 90 minutes. BFP-positive (stably transduced) cells were isolated on BD FACSAria II Cell Sorter, treated with 3μg/ml doxycycline for 7 days followed by treatment with 3μM imatinib for 2 days. 18 hours after exposing to 20 Gy IR, cells were processed as described above for the chromatin-bound RPA flow cytometry assay and analyzed on a BD FACSAria II Cell Sorter. Cells with high (top 10%), low (bottom 10%) RPA staining, as well as unsorted cells were collected, and genomic DNA of these cells were harvested for amplification of gRNAs.

To generate an Illumina sequencing library, gRNAs in the selected cells were first amplified using primers pKLV lib330F and pKLV lib490R and the program "98°C/5 minutes - [98°C/15 seconds - 60°C/15 seconds - 68°C/1 minute]x18 - 68°C/5 minutes". The resulting PCR products were used as the template for additional PCR amplification using primers PE.P5_pKLV lib195 Fwd and P7 index180 Rev and the program "94°C/5 minutes - [94°C/15 seconds - 60°C/30 seconds - 68°C/20 seconds]x10 - 68°C/5 minutes" to add Illumina HiSeq adapters and indexes (RPI5:CACTGT, RPI6: ATTGGC. RPI12: TACAAG). The final PCR products (~300 bp) were resolved in 1.5% agarose gel and purified by QIAQuick Gel Purification Kit (QIAGEN). Purified DNA was sequenced on

Illumina HiSeq2500 system to determine gRNA representation in each sample (50bp single-end reads).

Raw fastq files were demultiplexed by the Genomics and Epigenomics Core Facility of the Weill Cornell Medicine Core Laboratories Center. The gRNA sequence region was then retrieved from the sequencing data using Seqkit(Shen et al. 2016) and mapped to the gRNA sequence library(Koike-Yusa et al. 2014, Tzelepis et al. 2016). The number of reads of each library sequence was counted and then normalized as follows(Shalem et al. 2014):

$$\text{Normalized reads per gRNA} = \frac{reads\ per\ sgRNA}{total\ reads\ for\ all\ sgRNAs\ in\ sample} \times 10^6 + 1$$

Lastly, the enrichment score of a gRNA was calculated as a ratio of normalized reads of the gRNA in two samples.

pKLV lib330F: AATGGACTATCATATGCTTACCGT

pKLV lib490R CCTACCGGTGGATGTGGAATG

PE.P5_pKLV lib195 Fwd:

AATGATACGGCGACCACCGAGATCTGGCTTTATATATCTTGTGGAAAGGAC

744 P7 index180 Rev:

745 CAAGCAGAAGACGGCATACGAGAT*INDEX*GTGACTGGAGTTCAGACGTG

746 TGCTCTTCCGATCCAGACTGCCTTGGGAAAAGC

747

748 **Bulk gene inactivation:** To inactivate *53bp1*, *Lin37*, *CtIP*, *Brca1*, *Bard1*, *Blm*
749 or *Fancd2* in bulk cells populations, cells were transduced with lentivirus pKLV-
750 gRNAs by mixing cell suspensions with viral supernatant supplemented with
751 5μg/ml polybrene and 3μg/ml doxycline and spinning at 1,800 rpm for 90
752 minutes. Stably transduced cells were sorted 3 days after transduction and
753 sorted cells were kept in growth media with 3μg/ml doxycline for additional 24
754 hours before being subjected to analysis.

755

756 **Plasmid constructs:** pCW-Cas9 was a gift from Eric Lander & David Sabatini
757 (Addgene plasmid # 50661)(Wang et al. 2014). pX330-U6-Chimeric_BB-CBh-
758 hSpCas9 was a gift from Feng Zhang (Addgene plasmid # 42230)(Cong et al.
759 2013). pKLV-U6gRNA(BbsI)-PGKpuro2ABFP was a gift from Kosuke Yusa
760 (Addgene plasmid # 50946)(Koike-Yusa et al. 2014). pLenti-CMV-Blast-PIP-
761 FUCCI was a gift from Jean Cook (Addgene plasmid # 138715) (Grant et al.
762 2018).

763

For LIN37 reconstitution experiments, Lin37 WT or CD mutant were cloned into tetracycline-inducible TRE-Thy1.1 lentriviral vector to generate TRE-Lin37 (WT)-Thy1.1 or TRE-Lin37 (CD)-Thy1.1. WT Lin37 was amplified from Lin37 cDNA BC013546 (transOMIC) using primers Lin37 iso1_5'XhoI_S and Lin37 3'NotI_AS. To generate Lin37 CD mutant, Lin37 iso1_5'XhoI_S and Lin37 CD1_AS, and Lin37 CD2_S and 3'NotI_AS were first used to generate two cDNA fragments containing mutations in CD1 and CD2. The resulting PCR products were used in an overlapping PCR that annealed the two fragments to generate the full length Lin37 (CD) mutant.

Lin37 iso1_5'XhoI_S: GCCCTCGAGATGTTCCCGGTAAAGGTGAAAGTGG

Lin37 3'NotI_AS: GCCGCGGCCGCTCACTGCCGGTCATACATCTCCCGT

Lin37 CD1_AS:

TACAGTGGTGTGTTCTCACTGAACTGGGCCAAGTCCACAGCCCCG

GCAAATAGCTTGATC

Lin37 CD2_S:

ACTTGGCCCAGTTCAGTGAGAACACACCACTGTACCCCATCGCCGG

CGCCTGGATGCGCA

End-Seq: End-seq was performed as previously described, using $20x10^6$ abl pre-B cells harboring TET-inducible AsiSI-ER fusion treated with 3μM

785 imatinib(Canela et al. 2016). Briefly, cells were embedded in agarose plugs,
786 lysed, and treated with proteinase K and RNase A. The agarose-embedded
787 genomic DNA was then blunted using ExoVII (NEB) and ExoT (NEB). Blunted
788 DNA ends were A-tailed using Klenow exo- (NEB), and a biotinylated hairpin
789 adaptor BU1 was ligated. After adaptor ligation, DNA was recovered after plug
790 melting and treatment with beta-agarase. DNA was sheared to a length
791 between 150 and 200 bp by sonication (Covaris), and biotinylated DNA
792 fragments were purified using streptavidin beads (MyOne C1, Invitrogen).
793 Following streptavidin capture, the newly generated ends were end repaired
794 using T4 DNA polymerase, Klenow fragment, and T4 polynucleotide kinase; A-
795 tailed with Klenow exo-fragment (15 U); and finally ligated to hairpin adaptor
796 BU2 using the NEB Quick ligation kit. After the second adaptor ligation, libraries
797 were prepared by first digesting the hairpins on both adapters with USER
798 enzyme (NEB) then PCR amplified for 16 cycles using TruSeq index adapters.
799 All libraries were quantified using qPCR. Sequencing was performed on the
800 Illumina NextSeq500 (75 bp single-end reads).
801
802 END-seq reads were aligned to the mouse genome (GRCm38p2/mm10) using
803 Bowtie v1.1.2 with parameters (-n 3 -k 1 -l 50) and alignment files were
804 generated and sorted using SAMtools and BEDtools(Li et al. 2009, Quinlan and

Hall 2010, Langmead et al. 2009). Heatmap was plotted using heatmap.2 of gplots package in R.

BU1: 5'-Phos-GATCGGAAGAGCGTCGTGTAGGGAAAGAGTGUU[Biotin-dT]U[Biotin-dT]UUACACTCTTTCCCTACACGACGCTCTTCCGATC*T-3' [*phosphorothioate bond]

BU2: 5'-Phos-GATCGGAAGAGCACACGTCUUUUUUUUAGACGTGTGCTCTTCCGATC*T-3' [*phosphorothioate bond]

Antibodies for western blotting: The following antibodies were used for western blot analysis: 53BP1 (Bethyl Laboratories, A300-272A, 1:3000), LIN37 (Santa Cruz Biotechnology, sc-515686, 1:200), BLM (Bethyl Laboratories, A300-572A, 1:2000), BRCA1 for mouse (R&D Systems, gift from Dr. Andre Nussenzweig, NCI, 1:1000)(Zong et al. 2019), BRCA1 for human (Millipore Sigma, 07-434, 1:1000), RAD51(Millipore Sigma, ABE257, 1:2000), BARD1 (Thermo Fisher Scientific, PA5-85707, 1:1000), CtIP (gift from Dr. Richard Baer, Columbia University, New York), 1:1000), MRE11 (Novus Biologicals, NB100-142), RIF1 (Abcam, ab13422, 1:500), SHLD1/C20orf196 (Thermo Fisher Scientific, PA5-559280, 1:200), GAPDH (Sigma, G8795, 1:10000), KAP1 (Genetex, GTX102226, 1:2000), FANCD2 (R&D Systems, MAB93691, 1:1000),

826 BRCA2 for human (Proteintech, 19791-1-AP, 1:500), Rb1 (Thermo Fisher
827 Scientific, LF-MA0173, 1:1000), Phospho-Rb (Ser780) (Cell Signaling
828 Technology, 8180T, 1:1000), Phospho-Rb (Ser807/811) (Cell Signaling
829 Technology, 8516T, 1:1000), PCNA (Bethyl Laboratories, A300-276A,
830 1:3000).CDK4: (Novus Biologicals, NBP1-31308, 1:1000), CDK4 (phosphor
831 Thr 172): (GeneTex, GTX00778, 1:1000).
832
833 **RNA sequencing analysis**: RNA was purified from cycling *Lig4*$^{-/-}$ or *Lig4*
834 $^{-/-}$*:Lin37*$^{-/-}$ cells treated with imatinib for 72 hours (two biological replicates each)
835 using RNeasy mini kit (Qiagen). RNAseq libraries were prepared and
836 directional RNA sequencing of 2 × 50 bp performed at the Transcriptional
837 Regulation & Expression Facility at Cornell University using NextSeq 500
838 sequencer. The raw fastq reads were first processed with Trim-Galore
839 (Barbraham Institute). The filtered reads were then aligned to GRCm38
840 reference genome with ENSEMBL annotations using Spliced Transcripts
841 Alignment 2.7 (STAR 2.7)(Dobin et al. 2013). Differential expression was
842 computed using DESeq2 (Bioconductor) and a FDR 0.05 cutoff was used to
843 identify sets of differentially expressed genes (Love, Huber, and Anders 2014).
844
845 **Ionizing radiation-induced foci formation (IRIF) assay:** *Lig4*$^{-/-}$*, Lig4*$^{-/-}$*:Lin37*$^{-}$
846 $^{/-}$ and *Lig4*$^{-/-}$*:53bp1*$^{-/-}$ abl pre-B cells were treated or not with 3 μM imatinib for

847 48 hours. Thereafter, cells were pulsed with 10 μM EdU (Invitrogen) for 30
848 minutes and subjected to 10 Gy irradiation. For the detection of RAD51 foci,
849 irradiated cells were allowed to recover for 4 or 20 hours, at which point they
850 were immobilized on slides pre-coated with CellTak (Corning) and briefly pre-
851 extracted (20 mM HEPES, 50 mM NaCl, 3 mM $MgCl_2$, 0.3 M sucrose, 0.2%
852 Triton X-100) on ice for 15 seconds to remove soluble nuclear proteins.
853 Extracted samples were then fixed (4% paraformaldehyde), permeabilized
854 (0.5% Triton X-100 in PBS), incubated with anti-RAD51 primary antibody
855 (Abcam, ab176458, 1:250). Alternatively, irradiated (10 Gy) cells were allowed
856 to recover for 1 hour prior to fixation without a preceding pre-extraction step,
857 and subsequently incubated with primary antibodies recognizing 53BP1 (Novus
858 Biologicals, NB100-305,1:1000) or RIF1 (gift from Davide Robbiani (Rockefeller
859 University, New York),1:5000). In all cases, IRIFs were visualized by incubating
860 samples with Alexa Fluor 555-conjugated secondary antibodies (Invitrogen).
861 Where indicated, click-IT chemistry was performed as per manufacturer's
862 instructions. Finally, DNA was counterstained with DAPI (Thermo Fisher
863 Scientific). Immunofluorescence images were captured at 40X magnification on
864 a Lionheart LX automated microscope (BioTek Instruments, Inc.).
865 Quantification of IRIF was performed using the Gen5 spot analysis software
866 (BioTek).
867

gRNAs: Bulk gene inactivation or stable knockout mutants was achieved by CRSPR/Cas9 using the following gRNAs: *g53bp1* (GAACCTGTCAGACCCG ATC); *gLin37* (AAGCTATTTGACCGGAGTG); *gCtip* (ATTAACCGGCTACGA AAGA); *gBrca1* (GTCTACATTGAACTAGGTA); *gBard1* (AAATCGTAAAGGCT GCCAC); *gBlm* (GATTTAACGAAGGAATCGG); *gFancd2* (TCTTGTGATGTC GCTCGAC); *g53bp1* (*human*) (TCTAGTGTGTTAGATCAGG); *gLin37* (*human*) (TCTAGGGAGCGTCTGGATG).

Cell cycle phase purification by PIP-FUCCI: Abl pre-B cells or MCF10A cells were transduced with pLenti-CMV-Blast-PIP-FUCCI and selected in 5mg/ml Blasticidin for 3 days(Grant et al. 2018). To collect G_1 phase cells from proliferating cultures, mVenus-positive cells that were also mCherry-negative were sorted. To collect S/G_2/M cells, all mCherry-positive cells were sorted. Cell sorting was conducted on a BD FACSAria (BD Biosciences) at the Comprehensive Flow Cytometry Core at University of Alabama at Birmingham (supported by NIH P30 AR048311 and NIH P30 AI27667).

References

Bredemeyer, A. L., G. G. Sharma, C. Y. Huang, B. A. Helmink, L. M. Walker, K. C. Khor, B. Nuskey, K. E. Sullivan, T. K. Pandita, C. H. Bassing, and B. P. Sleckman. 2006. "ATM stabilizes DNA double-strand-break complexes during V(D)J recombination." *Nature* 442 (7101):466-70.

Bunting, S. F., E. Callen, N. Wong, H. T. Chen, F. Polato, A. Gunn, A. Bothmer, N. Feldhahn, O. Fernandez-Capetillo, L. Cao, X. Xu, C. X. Deng, T. Finkel, M. Nussenzweig, J. M. Stark, and A. Nussenzweig. 2010. "53BP1 inhibits homologous recombination in Brca1-deficient cells by blocking resection of DNA breaks." *Cell* 141 (2):243-54. doi: S0092-8674(10)00285-0 [pii]

10.1016/j.cell.2010.03.012.

Cai, M. Y., C. E. Dunn, W. Chen, B. S. Kochupurakkal, H. Nguyen, L. A. Moreau, G. I. Shapiro, K. Parmar, D. Kozono, and A. D. D'Andrea. 2020. "Cooperation of the ATM and Fanconi Anemia/BRCA Pathways in Double-Strand Break End Resection." *Cell Rep* 30 (7):2402-2415 e5. doi: 10.1016/j.celrep.2020.01.052.

Canela, A., S. Sridharan, N. Sciascia, A. Tubbs, P. Meltzer, B. P. Sleckman, and A. Nussenzweig. 2016. "DNA Breaks and End Resection Measured Genome-wide by End Sequencing." *Mol Cell* 63 (5):898-911. doi: 10.1016/j.molcel.2016.06.034.

Chang, H. H. Y., N. R. Pannunzio, N. Adachi, and M. R. Lieber. 2017. "Non-homologous DNA end joining and alternative pathways to double-strand break repair." *Nat Rev Mol Cell Biol* 18 (8):495-506. doi: 10.1038/nrm.2017.48.

Chapman, J. R., P. Barral, J. B. Vannier, V. Borel, M. Steger, A. Tomas-Loba, A. A. Sartori, I. R. Adams, F. D. Batista, and S. J. Boulton. 2013. "RIF1 is essential for 53BP1-dependent nonhomologous end joining and suppression of DNA double-strand break resection." *Mol Cell* 49 (5):858-71. doi: 10.1016/j.molcel.2013.01.002.

Ciccia, A., and S. J. Elledge. 2010. "The DNA damage response: making it safe to play with knives." *Mol Cell* 40 (2):179-204. doi: S1097-2765(10)00747-1 [pii] 10.1016/j.molcel.2010.09.019.

Cong, L., F. A. Ran, D. Cox, S. Lin, R. Barretto, N. Habib, P. D. Hsu, X. Wu, W. Jiang, L. A. Marraffini, and F. Zhang. 2013. "Multiplex genome engineering using CRISPR/Cas systems." *Science* 339 (6121):819-23. doi: 10.1126/science.1231143.

Dobin, A., C. A. Davis, F. Schlesinger, J. Drenkow, C. Zaleski, S. Jha, P. Batut, M. Chaisson, and T. R. Gingeras. 2013. "STAR: ultrafast universal RNA-seq aligner." *Bioinformatics* 29 (1):15-21. doi: 10.1093/bioinformatics/bts635.

Dorsett, Y., Y. Zhou, A. T. Tubbs, B. R. Chen, C. Purman, B. S. Lee, R. George, A. L. Bredemeyer, J. Y. Zhao, E. Sodergen, G. M. Weinstock, N. D. Han, A. Reyes, E. M. Oltz, D. Dorsett, Z. Misulovin, J. E. Payton, and B. P. Sleckman. 2014. "HCoDES reveals chromosomal DNA end structures with single-nucleotide resolution." *Mol Cell* 56 (6):808-18. doi: 10.1016/j.molcel.2014.10.024.

Escribano-Diaz, C., A. Orthwein, A. Fradet-Turcotte, M. Xing, J. T. Young, J. Tkac, M. A. Cook, A. P. Rosebrock, M. Munro, M. D. Canny, D. Xu, and D. Durocher. 2013. "A cell cycle-dependent regulatory circuit composed of 53BP1-RIF1 and BRCA1-CtIP

controls DNA repair pathway choice." *Mol Cell* 49 (5):872-83. doi: 10.1016/j.molcel.2013.01.001.

Forment, J. V., R. V. Walker, and S. P. Jackson. 2012. "A high-throughput, flow cytometry-based method to quantify DNA-end resection in mammalian cells." *Cytometry A* 81 (10):922-8. doi: 10.1002/cyto.a.22155.

Grant, G. D., K. M. Kedziora, J. C. Limas, J. G. Cook, and J. E. Purvis. 2018. "Accurate delineation of cell cycle phase transitions in living cells with PIP-FUCCI." *Cell Cycle* 17 (21-22):2496-2516. doi: 10.1080/15384101.2018.1547001.

Helmink, B. A., A. T. Tubbs, Y. Dorsett, J. J. Bednarski, L. M. Walker, Z. Feng, G. G. Sharma, P. J. McKinnon, J. Zhang, C. H. Bassing, and B. P. Sleckman. 2011. "H2AX prevents CtIP-mediated DNA end resection and aberrant repair in G1-phase lymphocytes." *Nature* 469 (7329):245-9. doi: nature09585 [pii] 10.1038/nature09585.

Henglein, B., X. Chenivesse, J. Wang, D. Eick, and C. Brechot. 1994. "Structure and cell cycle-regulated transcription of the human cyclin A gene." *Proc Natl Acad Sci U S A* 91 (12):5490-4. doi: 10.1073/pnas.91.12.5490.

Koike-Yusa, H., Y. Li, E. P. Tan, C. Velasco-Herrera Mdel, and K. Yusa. 2014. "Genome-wide recessive genetic screening in mammalian cells with a lentiviral CRISPR-guide RNA library." *Nat Biotechnol* 32 (3):267-73. doi: 10.1038/nbt.2800.

946 Langmead, B., C. Trapnell, M. Pop, and S. L. Salzberg. 2009. "Ultrafast and memory-efficient
947 alignment of short DNA sequences to the human genome." *Genome Biol* 10
948 (3):R25. doi: 10.1186/gb-2009-10-3-r25.
949 Li, H., B. Handsaker, A. Wysoker, T. Fennell, J. Ruan, N. Homer, G. Marth, G. Abecasis, R.
950 Durbin, and Subgroup Genome Project Data Processing. 2009. "The Sequence
951 Alignment/Map format and SAMtools." *Bioinformatics* 25 (16):2078-9. doi:
952 10.1093/bioinformatics/btp352.
953 Litovchick, L., S. Sadasivam, L. Florens, X. Zhu, S. K. Swanson, S. Velmurugan, R. Chen, M.
954 P. Washburn, X. S. Liu, and J. A. DeCaprio. 2007. "Evolutionarily conserved
955 multisubunit RBL2/p130 and E2F4 protein complex represses human cell cycle-
956 dependent genes in quiescence." *Mol Cell* 26 (4):539-51. doi:
957 10.1016/j.molcel.2007.04.015.
958 Love, M. I., W. Huber, and S. Anders. 2014. "Moderated estimation of fold change and
959 dispersion for RNA-seq data with DESeq2." *Genome Biol* 15 (12):550. doi:
960 10.1186/s13059-014-0550-8.
961 Mages, C. F., A. Wintsche, S. H. Bernhart, and G. A. Muller. 2017. "The DREAM complex
962 through its subunit Lin37 cooperates with Rb to initiate quiescence." *Elife* 6. doi:
963 10.7554/eLife.26876.
964 Malumbres, M., and M. Barbacid. 2001. "To cycle or not to cycle: a critical decision in cancer."
965 *Nat Rev Cancer* 1 (3):222-31. doi: 10.1038/35106065.

966 Mimitou, E. P., and L. S. Symington. 2009. "DNA end resection: many nucleases make light
967 work." *DNA Repair (Amst)* 8 (9):983-95. doi: 10.1016/j.dnarep.2009.04.017.
968 Mirman, Z., and T. de Lange. 2020. "53BP1: a DSB escort." *Genes Dev* 34 (1-2):7-23. doi:
969 10.1101/gad.333237.119.
970 Muljo, S. A., and M. S. Schlissel. 2003. "A small molecule Abl kinase inhibitor induces
971 differentiation of Abelson virus-transformed pre-B cell lines." *Nat Immunol* 4 (1):31-
972 7.
973 Muller, G. A., A. Wintsche, K. Stangner, S. J. Prohaska, P. F. Stadler, and K. Engeland. 2014.
974 "The CHR site: definition and genome-wide identification of a cell cycle transcriptional
975 element." *Nucleic Acids Res* 42 (16):10331-50. doi: 10.1093/nar/gku696.
976 Murina, O., C. von Aesch, U. Karakus, L. P. Ferretti, H. A. Bolck, K. Hanggi, and A. A. Sartori.
977 2014. "FANCD2 and CtIP cooperate to repair DNA interstrand crosslinks." *Cell Rep*
978 7 (4):1030-8. doi: 10.1016/j.celrep.2014.03.069.
979 Pennycook, B. R., and A. R. Barr. 2020. "Restriction point regulation at the crossroads
980 between quiescence and cell proliferation." *FEBS Lett*. doi: 10.1002/1873-
981 3468.13867.
982 Pierce, A. J., P. Hu, M. Han, N. Ellis, and M. Jasin. 2001. "Ku DNA end-binding protein
983 modulates homologous repair of double-strand breaks in mammalian cells." *Genes*
984 *Dev* 15 (24):3237-42. doi: 10.1101/gad.946401.

985 Prakash, R., Y. Zhang, W. Feng, and M. Jasin. 2015. "Homologous recombination and
986 human health: the roles of BRCA1, BRCA2, and associated proteins." *Cold Spring*
987 *Harb Perspect Biol* 7 (4):a016600. doi: 10.1101/cshperspect.a016600.
988 Quinlan, A. R., and I. M. Hall. 2010. "BEDTools: a flexible suite of utilities for comparing
989 genomic features." *Bioinformatics* 26 (6):841-2. doi: 10.1093/bioinformatics/btq033.
990 Rosenberg, N., D. Baltimore, and C. D. Scher. 1975. "In vitro transformation of lymphoid cells
991 by Abelson murine leukemia virus." *Proc Natl Acad Sci U S A* 72 (5):1932-6.
992 Sadasivam, S., and J. A. DeCaprio. 2013. "The DREAM complex: master coordinator of cell
993 cycle-dependent gene expression." *Nat Rev Cancer* 13 (8):585-95. doi:
994 10.1038/nrc3556.
995 Sartori, A. A., C. Lukas, J. Coates, M. Mistrik, S. Fu, J. Bartek, R. Baer, J. Lukas, and S. P.
996 Jackson. 2007. "Human CtIP promotes DNA end resection." *Nature* 450 (7169):509-
997 14. doi: nature06337 [pii]
998 10.1038/nature06337.
999 Setiaputra, D., and D. Durocher. 2019. "Shieldin - the protector of DNA ends." *EMBO Rep*.
1000 doi: 10.15252/embr.201847560.
1001 Shalem, O., N. E. Sanjana, E. Hartenian, X. Shi, D. A. Scott, T. Mikkelson, D. Heckl, B. L.
1002 Ebert, D. E. Root, J. G. Doench, and F. Zhang. 2014. "Genome-scale CRISPR-Cas9
1003 knockout screening in human cells." *Science* 343 (6166):84-87. doi:
1004 10.1126/science.1247005.

Shen, W., S. Le, Y. Li, and F. Hu. 2016. "SeqKit: A Cross-Platform and Ultrafast Toolkit for FASTA/Q File Manipulation." *PLoS One* 11 (10):e0163962. doi: 10.1371/journal.pone.0163962.

Symington, L. S., and J. Gautier. 2011. "Double-strand break end resection and repair pathway choice." *Annu Rev Genet* 45:247-71. doi: 10.1146/annurev-genet-110410-132435.

Tubbs, A. T., Y. Dorsett, E. Chan, B. Helmink, B. S. Lee, P. Hung, R. George, A. L. Bredemeyer, A. Mittal, R. V. Pappu, D. Chowdhury, N. Mosammaparast, M. S. Krangel, and B. P. Sleckman. 2014. "KAP-1 Promotes Resection of Broken DNA Ends Not Protected by gamma-H2AX and 53BP1 in G1-Phase Lymphocytes." *Mol Cell Biol*. doi: MCB.00441-14 [pii]
10.1128/MCB.00441-14.

Tzelepis, K., H. Koike-Yusa, E. De Braekeleer, Y. Li, E. Metzakopian, O. M. Dovey, A. Mupo, V. Grinkevich, M. Li, M. Mazan, M. Gozdecka, S. Ohnishi, J. Cooper, M. Patel, T. McKerrell, B. Chen, A. F. Domingues, P. Gallipoli, S. Teichmann, H. Ponstingl, U. McDermott, J. Saez-Rodriguez, B. J. P. Huntly, F. Iorio, C. Pina, G. S. Vassiliou, and K. Yusa. 2016. "A CRISPR Dropout Screen Identifies Genetic Vulnerabilities and Therapeutic Targets in Acute Myeloid Leukemia." *Cell Rep* 17 (4):1193-1205. doi: 10.1016/j.celrep.2016.09.079.

Unno, J., A. Itaya, M. Taoka, K. Sato, J. Tomida, W. Sakai, K. Sugasawa, M. Ishiai, T. Ikura, T. Isobe, H. Kurumizaka, and M. Takata. 2014. "FANCD2 binds CtIP and regulates

DNA-end resection during DNA interstrand crosslink repair." *Cell Rep* 7 (4):1039-47. doi: 10.1016/j.celrep.2014.04.005.

Wang, T., J. J. Wei, D. M. Sabatini, and E. S. Lander. 2014. "Genetic screens in human cells using the CRISPR-Cas9 system." *Science* 343 (6166):80-4. doi: 10.1126/science.1246981.

Weinberg, R. A. 1995. "The retinoblastoma protein and cell cycle control." *Cell* 81 (3):323-30. doi: 10.1016/0092-8674(95)90385-2.

Wyman, C., D. Ristic, and R. Kanaar. 2004. "Homologous recombination-mediated double-strand break repair." *DNA Repair (Amst)* 3 (8-9):827-33.

Zong, D., S. Adam, Y. Wang, H. Sasanuma, E. Callen, M. Murga, A. Day, M. J. Kruhlak, N. Wong, M. Munro, A. Ray Chaudhuri, B. Karim, B. Xia, S. Takeda, N. Johnson, D. Durocher, and A. Nussenzweig. 2019. "BRCA1 Haploinsufficiency Is Masked by RNF168-Mediated Chromatin Ubiquitylation." *Mol Cell* 73 (6):1267-1281 e7. doi: 10.1016/j.molcel.2018.12.010.